

Solar Energy

G. Oliveti, L. Marletta, N. Arcuri, M. De Simone, R. Bruno
and G. Evola

Abstract European Directive 2010/31/CE on energy efficiency in the buildings sector provides for significant actions for the reductions in energy consumption, and Directive RES 2009/28/CE stimulates the use of energy from renewable sources in order to meet such objectives. The chapter presents indications about the use of solar radiation for the energy requalification of buildings based on the results of research activities. Simplified evaluation methods are presented with the aim to verify the available potential energy, for the production of sanitary hot water, for winter heating and for the production of electrical energy, by means of systems, which use conventional solar collectors placed on the surfaces of the building shell, in particular on the roof slopes. In order to evaluate the energy improvement linked to the solar gain through the windows, the direct gain is evaluated by means of an accurate calculation model of the solar gains, which uses the coefficient of effective absorption of the entering radiation. With regard to sunspaces, some aspects of the thermal analysis, of the evaluation of the solar energy absorbed by the sunspace and by the adjacent room and of the benefits obtainable in terms of a reduction in the thermal requirements of the adjacent spaces are discussed. Finally, a discussion is presented regarding the possibility of using phase change materials (PCM) for the refurbishment of lightweight buildings. This technique allows for the improvement of the response of the building to solar gains, thus providing better thermal comfort in summer. In order to facilitate comprehension, the topics are supported by calculation methods and accompanied by numerical examples.

G. Oliveti · N. Arcuri (✉) · M. De Simone · R. Bruno
Department of Mechanical, Energy and Management Engineering,
University of Calabria, Cosenza, Italy
e-mail: natale.arcuri@unical.it

L. Marletta · G. Evola
Department of Industrial Engineering, University of Catania, Catania, Italy

Nomenclature

A_c	Collection surface area (m^2)
a_w	Azimuth ($^\circ$)
C_{eq}	Equivalent specific heat capacity of PCM (J/kg K)
c_p	Specific heat of the air (J/kg K)
\bar{E}_{ass}	Daily average monthly solar energy absorbed by an internal space (J)
E_i	Daily average monthly energy incident on the external glazed surface (J/m^2)
f	Glazed fraction of a wall (-)
f_c	Corrective factor (-)
F_R	Removal factor of the thermal collector (-)
F'	Efficiency factor of the thermal collector (-)
g	Total solar gain for normal incidence of the glazed system (-)
G_c	Solar global irradiation on a surface (W/m^2)
G_e	Solar power entering in an environment through the glazed surface (W/m^2)
h_c	Convective thermal exchange coefficient ($W/m^2 K$)
I_{bo}	Direct solar irradiation on the horizontal plane (W/m^2)
I_{do}	Diffuse solar irradiation on the horizontal plane (W/m^2)
\dot{m}_v	Ventilation flow rate (kg/s)
P_{cel}	Electrical power supplied by the PV cell (W)
Q_{ai}^+	Heat transferred by convection to the internal air (J)
Q_i	Incident solar energy on the sunspace shell (J)
Q_{ass}	Solar power absorbed by the internal environment, or net solar gain (W)
$Q_{as,s}$	Solar energy absorbed in the sunspace (J)
Q_p	Lost thermal power of solar collector (W)
Q_{sol}	Daily average monthly solar gain through the glazed surfaces (J)
Q_{tr}	Transmitted solar energy through the sunspace shell (J)
Q_u	Useful thermal power of solar collector (W)
R_b	Inclination factor of direct solar radiation (-)
\bar{R}_b	Monthly direct radiation inclination factor (-)
R_d	Inclination factor of diffuse solar radiation (-)
R_r	Inclination factor of reflected solar radiation (-)
T_a	Outdoor air temperature (K)
T_{as}	Air temperature in the sunspace (K)
T_c	Average temperature of the PV cell or panel (K)
T_i	Internal surface temperature (K)
T_p	Peak melting temperature of PCM (K)
\bar{T}_p	Average temperature of the thermal solar collector absorbent plate (K)
U	Thermal transmittance ($W/m^2 K$)

Greek Symbols

α	Absorption coefficient of solar radiation (-)
α_{cav}	Effective absorption coefficient of the internal environment (-)

α_i	Absorption coefficient in the solar band of the i th surface (-)
α_f	Solar absorption coefficient of the floor and of the walls (-)
α_m	Average absorption coefficient of the opaque surfaces of the internal environment (-)
α_s	Effective absorption coefficient of the sunspace (-)
α_w	Solar absorption coefficient of the walls (-)
β	Inclination ($^\circ$)
Δt	Time interval (s)
η	Efficiency (-)
η_u	Utilisation factor (-)
$\eta_{u,v}$	Utilisation factor imputable to ventilation (-)
τ	Transmission coefficient of solar radiation (-)
τ_b	Transmission coefficient of the direct solar radiation of the glazed system (-)
τ_d	Transmission coefficient of the diffuse solar radiation of the glazed system (-)
τ_g	Transmission coefficient of the reflected solar radiation of the glazed system (-)
ψ	Glazed fraction of the room (-)

1 General Considerations of the Use of Solar Thermal Energy

In energy requalification interventions on buildings, solar energy can be used with active systems in which the transport of the energy collected is carried out with fluids in movement under the action of pumps or fans, or even the use of passive systems, in which collection and storage can be combined in a sole component and energy transfer is entrusted to thermal irradiation and to transport due to natural convection, without the contribution of auxiliary energy.

In active systems, solar radiation is used for the heating of a thermo-vector fluid by means of a particular heat exchanger which is the solar collector. Such a component transforms radiant energy into thermal energy which is then used for many different aims, but mainly for winter heating and for the production of domestic hot water (DHW).

Besides the solar collector, due to the precariousness and discontinuity of the solar source, these systems are equipped with one or more storage tanks with water, which store the surplus thermal energy in order to return it, upon the user's request, at different periods.

With water plants, the heating of environments requires the use of low-temperature emission terminals, such as radiant panels or fan coils, in which the efficiency of solar collection is much higher when the required temperature for the thermo-vector fluid is lower.

In order for solar plants to be financially convenient, they must be dimensioned in such a way as to supply only a fraction of the energy thermal requirement, while the remaining part is supplied by an auxiliary system. The correct sizing of such

plants requires economic evaluation and optimisation methods of the system formed by the solar plant and by the integration system. The main project parameter is represented by the area of collectors A_c : with an increase in the collection area, the collected energy and energy saving increases, but, at the same time, the cost of the plant increases. In order to realise a solar plant, high investment costs are required, which must be addressed prior to starting the plant, and low operating costs which are renewed each year. Economic evaluations are obtained through an analysis of the costs and the gains for the entire life of the plant, updating expenditure and income over several years.

The optimal dimension of the investment can be obtained by determining the value of the collection area which renders the maximum net present value (NPV), or by means of optimisation methods such as the global cost method and the global saving method. The economic variable, such as the global cost of the plant or the global saving obtained, defined as the difference between the global cost of the conventional plant which uses usual sources and the global cost of an integrated solar plant, is expressed as the function of the area of collectors. Such an area is determined in such a way as to maximise or minimise the chosen economic function. In the global cost method of an integrated solar system, the cost relating to the conventional integration plant is not considered in which it is supposed that the latter must be present in every case.

2 Thermal Analysis of Solar Collectors

Thermal solar collectors are simple devices. The flat type, which is the most common and the most economic, is formed by a radiation collection plate, by one or more glass coverings, in order to reduce thermal loss externally, as well as a system of channels connected to the plate through which a thermo-vector fluid flows to remove power. A containment box completes the structure in which the rear and lateral insulation of the panel is inserted.

The instantaneous thermal balance equation of the absorbent plate in stationary regime conditions can be expressed as

$$G_c A_c (\tau\alpha) = Q_u + Q_p \quad (1)$$

with G_c global irradiation incident on the collector (W/m^2), $(\tau\alpha)$ effective product of the transmission coefficient of the glazed covering system and the absorption coefficient of the absorbent black plate, A_c collection surface area, Q_u useful power delivered by the plate to the thermo-vector fluid and Q_p thermal power lost due to convection and irradiation by the collector to the external environment.

The power lost is evaluated with the relation:

$$Q_p = U_c A_c (\bar{T}_p - T_a) \quad (2)$$

with U_c global thermal exchange coefficient between the plate and the air, \bar{T}_p average temperature of the absorbent plate and T_a outdoor air temperature.

Through relations (1) and (2), the useful power can be expressed as the difference between the power absorbed and the power lost:

$$Q_u = G_c A_c \tau \alpha - U_c A_c (\bar{T}_p - T_a) \quad (3)$$

Efficiency is the parameter used to thermally qualify the collector. The instantaneous efficiency η of the collector is defined as the relation between the useful power and the incident solar power:

$$\eta = \frac{Q_u}{G_c A_c} \quad (4)$$

The average efficiency in a time interval (an hour, a day, a month) is defined by means of the equation:

$$\eta = \frac{\int_t^{t+\Delta t} Q_u(t) dt}{\int_t^{t+\Delta t} A_c G_c dt} \quad (5)$$

The expression (3) does not allow for the calculation of the useful power Q_u , given that the average temperature of the absorbent plate is not known. The plate is the seat of a bidirectional temperature distribution, in the flow rate direction within the channels and in a perpendicular direction; the determination of which allows the calculation of the power that is transferred by the plate to the cooling liquid.

In the thermal analysis of the solar collectors, the collector efficiency factor F' and the heat removal factor F_R are defined [1, 2]. The physical meaning of the former factors is the following: F' represents the relation between the thermal resistance between the absorbent plate and the external environment, in the hypothesis of uniform plate temperature, and the thermal resistance between the fluid flowing in the channels and the external environment, F_R is the ratio between the power taken by the cooling flow rate and the power that should be taken by it were the plate to have uniform temperature and equal to the inlet temperature of the fluid. This power is the maximum transferable to the fluid since in the considered conditions, the power lost is minimal.

The introduction of factors F' and F_R allows for the expression of the useful thermal power transferred to the flow rate with the relations:

$$Q_u = F' A_c [(\tau \alpha) G_c - U_c (\bar{T}_f - T_a)] \quad (6)$$

$$Q_u = F_R A_c [(\tau \alpha) G_c - U_c (T_{fi} - T_a)] \quad (7)$$

Equation (7) consents the direct calculation of the useful power, given that the inlet temperature of the fluid is commonly known, unlike (6) in which the average temperature appears, which is generally not known, given that the outlet temperature of the water flow rate is not known. For such a reason, in this case, the resolution is obtained by successive iteration: the editing temperature is set and from (6) the useful power is obtained, and by means of the water flow rate heating equation:

$$Q_u = \dot{m} c_p (T_{fu} - T_{fi}) \quad (8)$$

the new outlet temperature is obtained.

Table 1 Typical coefficients of the efficiency curve for different types of thermal solar collectors

Collector type	$F'(\tau\alpha)$	$F'U_{co}$ (W/m ² K)	$k \cdot F'$ (W/m ² K ²)
Unglazed	0.770	9.215	0.700
Flat with one glass covering	0.810	4.360	0.650
Flat with two glass coverings	0.755	2.725	0.095
Selective with one glass	0.840	3.550	0.500
Evacuated tube	0.641	1.059	0.004
Evacuated heat pipe	0.765	0.390	0.002

3 Efficiency Curves of Solar Collectors

Commonly used solar collectors are of different types, and the choice of the most suitable model to be used is dependent, above all, on the required temperature levels, on the thermal energy requirements and also on the period of use during the year [3]. The main collectors available on the market are as follows: unglazed solar collectors, glazed collectors, glazed collectors with selective surfaces, evacuated tube collectors and evacuated heat pipe solar collectors.

If one considers the expression of efficiency (6), in which the average temperature of the fluid between entering and exiting the collector appears, and the most realistic hypothesis is adopted of the coefficient of loss of the collector is not constant but varies in a linear manner in relation to temperature differences:

$$U_c = U_{co} + k(\bar{T}_f - T_a) \quad (9)$$

k is a constant value, the expression becomes

$$\eta = F'(\tau\alpha) - F'U_{co} \frac{\bar{T}_f - T_a}{G_c} - k \cdot F' \frac{(\bar{T}_f - T_a)^2}{G_c} \quad (10)$$

In Table 1, the values assumed by the coefficients $F'(\tau\alpha)$, $F'U_{co}$, and $k \cdot F'$ are reported for the main types of collectors [28].

4 Solar Plants

4.1 Introduction

These plants, due to reasons of technical–economical feasibility, are sized to cover a fraction of the energy thermal requirement. From that, it is necessary to equip them with a traditional integration system (boiler or electrical resistance) in order to cover the remaining requirement fraction. Furthermore, due to climatic variability, a water storage tank is always present [4]. For the production of DHW, the most simple plant is that with natural circulation, characterised by the placing of the tank in a higher position compared to the collector.

If it is not possible to place the storage tank higher than the collector, then it will be necessary to resort to forced circulation. A pump placed on the cold branch of the circuit provides for the circulation of the fluid between the storage system and the collector. Forced circulation plants can be equipped with two storage tanks, the first for “preheating” at more limited temperatures in order to improve collection efficiency and the second for “use” interfaced to the auxiliary system.

The installation of solar plants in condominium buildings is more convenient compared to their installation in single residential units. The collectors can be placed on roof slopes, and integration with the existing plant does not usually present any particular difficulties.

These plants can either use natural or forced circulation. In the first case, it is necessary to install monoblock systems in which each panel supplies DHW to a single residential unit. Many gas boilers used for domestic heating and for the production of DHW are semi-modulating and supply a minimum thermal power of 4–5 kW, independently of the inlet water flow rate temperature. Such a power can result as being excessive to obtain the requested outlet temperature of 45 °C. In order to remedy such an inconvenience, it is good practice to install a mixing valve before the boiler which reduces the hot water flow rate taken from the tank and, by means of a cold water flow rate originating from the aqueduct network, reduces the temperature entering the boiler.

In the case in which condensation boilers are used, the supply of minimum power leads to higher generation efficiency due to the use of the heat from condensation present in fumes.

The centralised production of DHW by means of forced circulation plants equipped with a sole service storage system for all the condominium users results as being more rational. This solution is capable of producing significant fractions of the DHW thermal requirement and is easy to integrate with existent plants since it requires a hot water distribution system which is realisable with a single pipe to which all users can be connected.

In water plants for the heating of buildings, the most efficient use of solar radiation is obtained using a low-temperature water flow rate (40–50 °C) with suitable energy distribution systems for the spaces to be heated, such as radiant floors, radiant ceilings, or fan-coil-type devices. The solar plant and the integration system can be configured differently compared to the environment to be heated: the solar plant and the boiler are placed in parallel, or in series, the solar panels and the integration system jointly supply the storage system, or even the solar and the auxiliary are independent with a double distribution system of heat to the spaces. The latter configuration lends itself to being used in buildings that are already equipped with traditional heating plants with radiators.

4.2 Planning Methods of Solar Plants

In order to plan solar plants in an accurate manner, it is necessary to simulate the plant components, such as the array of collectors, the storage system, the heat exchangers, the distribution network, the distribution terminals and the control system, with dynamic models. The equations to consider are those of conservation of the mass and energy for the various plant components.

Often simplified models based on energetic type evaluations whose level of accuracy depends on the entity of simplification are used. For example, the average annual method [3] neglects the dynamic interaction between the storage tank, the field of collectors and the heat use system and for such reasons provides preliminary evaluations. More accurate results are obtained with the f -chart method [2] created based on the results of numerous dynamic simulations of reference solar plants.

Several f -chart versions are available: for forced circulation liquid plants for the heating of spaces and production of DHW; for plants which are solely for the production of DHW; for natural circulation liquid plants and also for air plants. Such a method allows for the calculation of the fraction f of the monthly thermal requirement obtained from the solar radiation in a plant with determined properties and the annual solar fraction F . It is a verification method of plant performance which, if opportunely used, allows for the obtainment of an optimal plant design.

Hereafter, two simplified calculation procedures are described. The first regards DHW production plants and the second plants for heating, both regarding existing buildings. The two procedures use roof-covering slopes as sunlight surface, which are differently tilted and oriented, and evacuated heat pipe solar collectors.

4.3 A Simplified Method for the Determination of the Solar Collector Surface of Buildings for the Production of DHW with Evacuated Heat Pipe Collectors

In new buildings, and in those subject to important restructuring work, it is good practice to expect that not less than 50 % of the annual thermal energy requirement for DHW is produced by solar collectors.

The considered method [5] provides for the use of evacuated heat pipe collectors. If used to produce a water flow rate at a temperature of 35–50 °C, these collectors' deliver performance is mainly dependent on solar radiation, while the influence of the temperature difference between the thermo-vector fluid and the external air can be held to be negligible. In such conditions, collectors' efficiency is independent from the storage temperature and therefore from the thermal energy removing from such a component.

The estimation of producible thermal energy of DHW plants (kWh/m²), with panels that are arbitrarily oriented and tilted, can be determined with a simplified

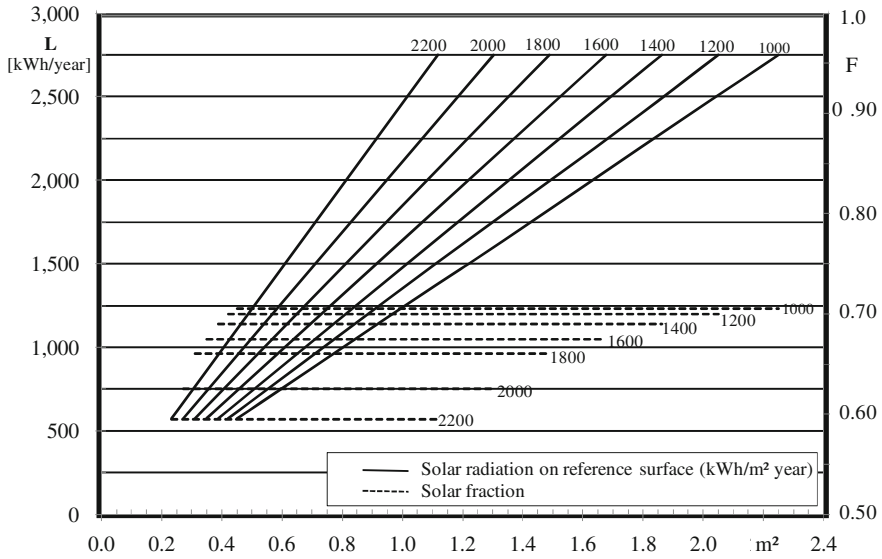


Fig. 1 Collection area and solar fraction as a function of the annual thermal energy requirement for DHW and of the annual solar energy on the reference surface ($\beta = 30^\circ$, $a_w = 0^\circ$). Small residential users

procedure which uses results obtained in reference plants with south-facing collection surfaces ($a_w = 0^\circ$) and tilted by 30° ($\beta = 30^\circ$).

Such an arrangement generally provides the best annual collection conditions for latitudes between 35°N and 45°N .

If the slopes of the roof covering of a building are used as the collection surface, which are generally differently oriented and tilted, the method assigns each slope with a thermal producibility value determined from the value relative to reference setting. In such a way, it is possible to define the best positioning of the collection surface and the area necessary to obtain the same thermal requirement fraction.

The data required by the calculation procedure are the DHW annual thermal energy requirement (kWh/year) and the annual solar energy (kWh/(m² year)) incident on a unitary reference surface ($\beta = 30^\circ$; $a_w = 0^\circ$).

Through these data and the graphs in Figs. 1 and 2, it is possible to obtain the collection area and the annual fraction of the thermal requirement provided by the solar source. The annual energy values on the reference plane are variable from 1,000 to 2,200 kWh/(m² year) corresponding to the geographic area comprised between the Northern Africa and the northern Europe. Figure 1 relates to small domestic users with annual thermal requirements of less than 3,000 kWh/year, while Fig. 2 relates to larger thermal requirements, though not greater than 45,000 kWh/year.

In order to calculate the storage volume, if L is the DHW annual thermal requirement, the following relation is used (L in kWh and V in litres):

$$V = 0.068 L \tag{11}$$

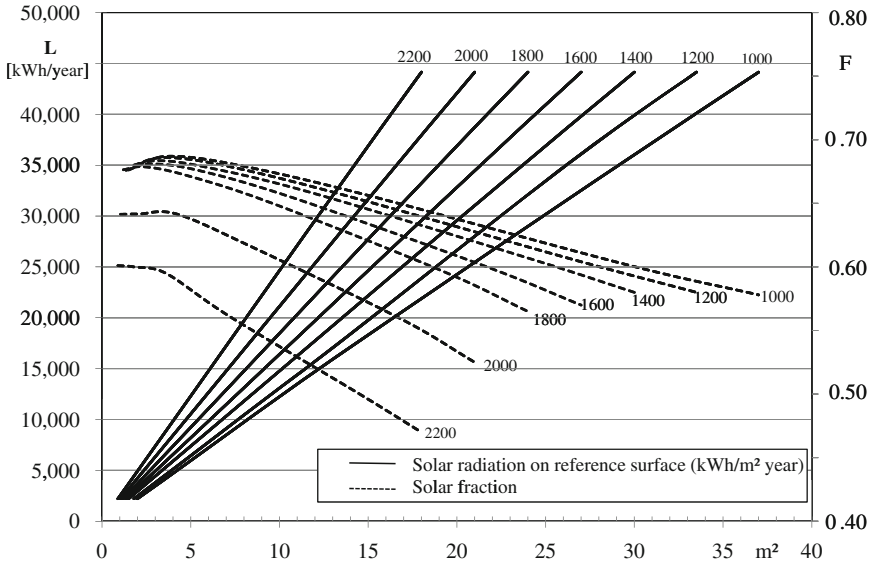


Fig. 2 Collection area and annual solar fraction as a function of the thermal energy requirement for DHW and of the radiation on the reference surface ($\beta = 30^\circ$, $a_w = 0^\circ$). Large residential users

For example, for an annual thermal requirement of 2,500 kWh and an availability of solar radiation on the reference surface of 1,600 kWh/m², from Fig. 1, a collection surface of 1.2 m² is obtained and an annual solar fraction of the DHW thermal requirement of 0.62 is obtained. Annual thermal producibility is equal to $0.62 \cdot 2,500/1.2 = 1,292$ kWh/(m² year).

For collection surfaces which are differently oriented and tilted, the calculation procedure provides coefficients of reduction in the annual producibility relative to the reference layout. Table 2 shows the corrective coefficients relating to 42°N of latitude for collection surfaces with β variable between 0° and 90° and azimuth angles a_w variable between 0° (south) and 180° (north). Such coefficients can be held to be valid for latitudes between 35°N and 45°N with an acceptable error of less than 3 %.

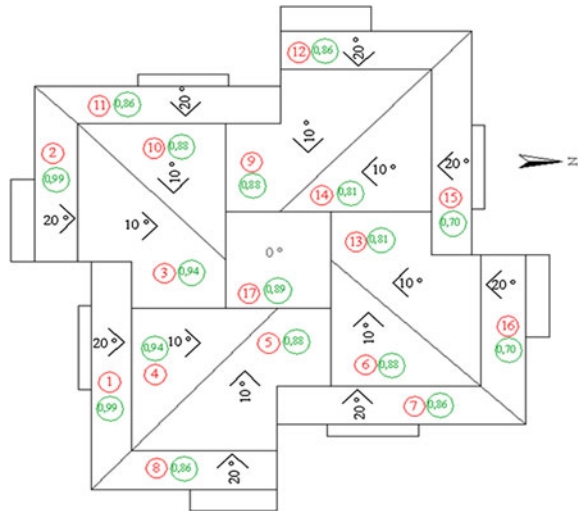
For example, for an east-facing surface ($a_w = 90^\circ$) with $\beta = 40^\circ$, the corrective factor of annual thermal producibility is equal to 0.79. If one considers the thermal requirement and the availability of solar radiation of the previous example for the reference setting, the producibility of the considered surface becomes $0.79 \cdot 1,292 = 1,021$ kWh/year. In order to obtain the same solar fraction of the requirement, a collection surface equal to $0.62 \cdot 2,500/1,021 = 1.5$ m² is required.

Example 1 Figure 3 shows the roof covering of a condominium building in Rome. On each slope, the reference number, orientation, inclination and corrective factor of the annual thermal producibility, determined by means of Table 2, are reported.

Table 2 Corrective factors f_c of the annual thermal energy on the reference surface varying the inclination β and the azimuth angle a_w of the collection surface

β (°) → a_w (°) ↓	0	10	20	30	40	60	90
0	0.89	0.94	0.99	1.00	0.99	0.90	0.64
22.5	0.89	0.95	0.98	0.99	0.97	0.89	0.64
45	0.89	0.93	0.95	0.95	0.93	0.84	0.62
67.5	0.89	0.91	0.91	0.90	0.87	0.78	0.57
90	0.89	0.88	0.86	0.83	0.79	0.69	0.51
112.5	0.89	0.86	0.82	0.76	0.71	0.60	0.44
135	0.89	0.84	0.77	0.70	0.63	0.50	0.36
157.5	0.89	0.83	0.74	0.65	0.57	0.42	0.30
180	0.89	0.81	0.70	0.64	0.55	0.39	0.28

Fig. 3 Roof geometry with an indication of the orientation, inclination and the annual productivity corrective factor



The sizing of collection surface of a centralised plant for the production of DHW for an annual thermal energy requirement of 44,200 kWh which uses evacuated heat pipe solar collectors is required. The annual incident radiation on the reference surface ($a_w = 0^\circ$, $\beta = 30^\circ$) is equal to 1,800 kWh/m² year. The use of modules with a collection surface equal to 2.0 m² is supposed.

Considering the reference setting, for a requirement of 44,200 kWh/year and an incident radiation of 1,800 kWh/m² year, the graphic in Fig. 2 provides a collection surface of 24 m² and a solar fraction of the requirement of 56 %. The annual thermal producibility results as being equal to 0.56 · 44,200/24 = 1,031 kWh/m².

If collectors, each with a surface area equal to 2 m² are used, in the hypothesis that the roof surface which can effectively be used is equal to 50 % of the effective

Table 3 Results for 17 slope calculations

Slope N.	a_w (°)	β (°)	Area (m ²)	Effective area (m ²)	f_c	Producibility (kWh/m ² year)	Installable collectors	Energy produced (kWh/year)	
S	1	0	20	36.5	18.3	0.99	1021	9	18,372
	2	0	20	27.7	13.9	0.99	1021	6	12,248
	3	0	10	56.9	28.5	0.94	969	14	27,136
	4	0	10	40.5	20.3	0.94	969	10	19,383
HZ	17	–	0	39.1	19.6	0.89	918	9	16,517
E	5	90	10	52.1	26.1	0.88	907	13	23,589
	6	90	10	36.6	18.3	0.88	907	9	16,331
W	9	90	10	58.4	29.2	0.88	907	14	25,404
	10	90	10	39.1	19.6	0.88	907	9	16,331
E	7	90	20	36.9	18.5	0.86	887	9	15,960
	8	90	20	29.4	14.7	0.86	887	7	12,413
W	11	90	20	37.3	18.7	0.86	887	9	15,960
	12	90	20	29.4	14.7	0.86	887	7	12,413
N	13	180	10	56	28	0.81	835	14	23,383
	14	180	10	42	21	0.81	835	10	16,702
	15	180	20	36.6	18.3	0.70	722	9	12,991
	16	180	20	30.8	15.4	0.70	722	7	10,104

surface due to obstructions linked to the very complex roof geometry, the collection results obtainable are reported in Table 3. For each of the 17 slopes, the azimuth a_w , the inclination β , the slope surface, the usable slope surface, the corrective factor f_c of producibility, the producibility of each slope, the number of installed collectors and the energy produced are reported.

The table allows for the evaluation of all the possible solutions in order to meet the thermal requirement. For example, the use of slope n°1 and slope n°2 with a total collection surface equal to 22 m² (9 collectors on slope n°1 and 2 on slope n°2) is sufficient to satisfy 50 % of the thermal energy required for the production of DHW ($1,021 \cdot 22 = 22,462$ kWh). Alternatively, the production of DHW can be guaranteed using the entire available surface of slope n°3, or n°5.

4.4 A Simplified Method for the Determination of Solar Energy Utilisable for Integration in Winter Heating

The former procedure can be extended to determine the solar energy utilisable each month, integrated by the energy supplied by the heating plant, in order to meet the monthly energy requirements. Evacuated heat pipe collectors are also used in this case for the production of thermal energy at a temperature of 40–50 °C situated on the slope surfaces of the roof covering. For each month of heating, given that the monthly energy incident on the reference surface is known

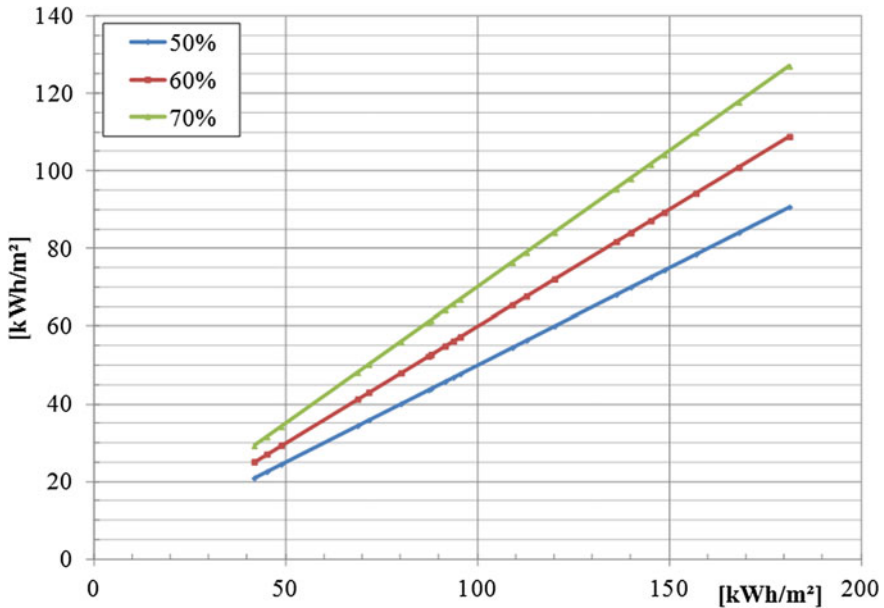


Fig. 4 Monthly energy utilisable as a function of the incident monthly energy on the reference surface ($a_w = 30^\circ$; $\beta = 0^\circ$) for three values of collector thermal efficiency

($a_w = 30^\circ$; $\beta = 0^\circ$), by means of the graphic in Fig. 4, it is possible to evaluate the monthly thermal energy available for heating (kWh/m^2), for three different values of the average monthly efficiency of the collector. For intermediate efficiency values, the energy produced can be evaluated for linear interpolation.

Given the known monthly energy utilisable on the reference plane, the utilisable energy on any tilted and oriented surface, for example on a roof covering, can be evaluated by applying monthly corrective factors reported in Table 4. Starting from the utilisable monthly energy per area unit and from the available collection areas, it is possible to determine the monthly and seasonal energy that can be used to integrate the thermal energy requirements necessary for winter heating.

5 Photovoltaic System

The vertical elements of the building shell and, even better, the covering roof surfaces can be validly used for the production of electrical energy through photovoltaic panels, to be used for the functioning of building conditioning plants and systems, with a consequent reduction in electrical energy taken from the grid.

In a photovoltaic cell, the absorbed solar power is only in part transformed into electrical power, while the rest is lost towards the outside as thermal power. The

Table 4 Corrective factors f_c of the monthly utilisable energy on the reference surface varying the inclination β and the azimuth angle a_w of the collection surface

		Inclination β (°)						
		0	10	20	30	40	60	90
<i>October</i>								
Azimuth a_w (°)	0	0.79	0.88	0.95	1.00	1.03	1.01	0.82
	22.5	0.79	0.87	0.94	0.98	1.00	0.98	0.78
	45	0.79	0.85	0.90	0.92	0.93	0.89	0.70
	67.5	0.79	0.82	0.84	0.84	0.83	0.77	0.59
	90	0.79	0.79	0.77	0.75	0.71	0.64	0.48
	112.5	0.79	0.75	0.70	0.64	0.59	0.50	0.37
	135	0.79	0.72	0.63	0.55	0.48	0.38	0.29
	157.5	0.79	0.69	0.58	0.48	0.39	0.31	0.25
	180	0.79	0.68	0.57	0.44	0.34	0.30	0.25
<i>November</i>								
Azimuth a_w (°)	0	0.72	0.83	0.93	1.00	1.05	1.08	0.94
	22.5	0.72	0.82	0.91	0.97	1.01	1.03	0.88
	45	0.72	0.79	0.85	0.89	0.91	0.89	0.73
	67.5	0.72	0.76	0.78	0.78	0.78	0.73	0.57
	90	0.72	0.71	0.69	0.66	0.64	0.56	0.43
	112.5	0.72	0.66	0.61	0.55	0.51	0.43	0.32
	135	0.72	0.63	0.53	0.46	0.40	0.33	0.26
	157.5	0.72	0.60	0.48	0.39	0.34	0.31	0.25
	180	0.72	0.59	0.46	0.36	0.34	0.31	0.25
<i>December</i>								
Azimuth a_w (°)	0	0.67	0.80	0.91	1.00	1.07	1.13	1.02
	22.5	0.67	0.79	0.89	0.98	1.04	1.09	0.97
	45	0.67	0.76	0.84	0.90	0.94	0.95	0.82
	67.5	0.67	0.72	0.76	0.78	0.79	0.76	0.62
	90	0.67	0.67	0.66	0.65	0.63	0.57	0.44
	112.5	0.67	0.62	0.57	0.52	0.48	0.41	0.31
	135	0.67	0.57	0.48	0.41	0.37	0.31	0.25
	157.5	0.67	0.54	0.42	0.35	0.33	0.30	0.25
	180	0.67	0.53	0.40	0.34	0.33	0.30	0.25
<i>January</i>								
Azimuth a_w (°)	0	0.70	0.82	0.92	1.00	1.06	1.10	0.98
	22.5	0.70	0.81	0.90	0.97	1.02	1.05	0.91
	45	0.70	0.78	0.84	0.89	0.92	0.91	0.76
	67.5	0.70	0.74	0.76	0.78	0.77	0.73	0.57
	90	0.70	0.69	0.67	0.65	0.62	0.56	0.42
	112.5	0.70	0.64	0.59	0.53	0.49	0.41	0.31
	135	0.70	0.60	0.51	0.44	0.39	0.33	0.26
	157.5	0.70	0.58	0.46	0.38	0.35	0.32	0.26
	180	0.70	0.57	0.44	0.36	0.35	0.32	0.26

(continued)

Table 4 (continued)

		Inclination β ($^\circ$)						
		0	10	20	30	40	60	90
<i>February</i>								
Azimuth a_w ($^\circ$)	0	0.75	0.86	0.94	1.00	1.04	1.05	0.88
	22.5	0.75	0.85	0.92	0.97	1.01	1.00	0.83
	45	0.75	0.82	0.87	0.91	0.92	0.89	0.72
	67.5	0.75	0.79	0.81	0.81	0.81	0.75	0.59
	90	0.75	0.75	0.73	0.71	0.68	0.61	0.46
	112.5	0.75	0.70	0.65	0.60	0.55	0.47	0.35
	135	0.75	0.67	0.58	0.50	0.44	0.36	0.28
	157.5	0.75	0.65	0.53	0.43	0.36	0.31	0.26
	180	0.75	0.64	0.51	0.39	0.34	0.31	0.26
<i>March</i>								
Azimuth a_w ($^\circ$)	0	0.84	0.92	0.97	1.00	1.01	0.96	0.74
	22.5	0.84	0.91	0.96	0.98	0.99	0.93	0.71
	45	0.84	0.89	0.92	0.94	0.93	0.86	0.66
	67.5	0.84	0.87	0.87	0.87	0.85	0.78	0.59
	90	0.84	0.84	0.82	0.79	0.76	0.67	0.51
	112.5	0.84	0.81	0.76	0.71	0.66	0.56	0.41
	135	0.84	0.78	0.70	0.63	0.55	0.44	0.33
	157.5	0.84	0.76	0.66	0.56	0.47	0.35	0.28
	180	0.84	0.75	0.65	0.53	0.42	0.32	0.27
<i>April</i>								
Azimuth a_w ($^\circ$)	0	0.94	0.98	1.00	1.00	0.98	0.87	0.59
	22.5	0.94	0.97	0.99	0.99	0.96	0.86	0.59
	45	0.94	0.96	0.97	0.96	0.93	0.83	0.60
	67.5	0.94	0.95	0.94	0.92	0.88	0.78	0.58
	90	0.94	0.93	0.90	0.86	0.82	0.72	0.53
	112.5	0.94	0.91	0.86	0.80	0.75	0.63	0.47
	135	0.94	0.89	0.82	0.75	0.67	0.53	0.39
	157.5	0.94	0.88	0.80	0.71	0.61	0.44	0.32
	180	0.94	0.88	0.80	0.70	0.59	0.38	0.29

equation of the instantaneous thermal balance in a stationary regime can be placed in form [2]

$$P_{\text{cel}} = A_c G_c \tau \alpha - A_c U_c (T_c - T_a) \tag{12}$$

where P_{cel} is the electrical power supplied by the cell, $\tau \alpha$ produced by the transmission coefficient of the radiation through the covering system and the absorption coefficient of the cell, U_c the coefficient of the thermal exchange between the cell and the external environment, T_c the average temperature of the cell and T_a the external air temperature.

The cell efficiency is defined as the relation between the electrical power generated and the incident solar irradiance:

$$\eta_c = \frac{P_c}{A_c G_c} \quad (13)$$

Replacing (12) with (13), the following is obtained:

$$\eta_c = \tau\alpha - \frac{U_c(T_c - T_a)}{G_c} \quad (14)$$

If one considers a module, formed by several cells which are electrically connected and closed in a sealed container, or a panel, made from more connected models and assembled in a rigid structure, for a total area A and formed by n cells, the efficiency is written in the following form:

$$\eta_c = \frac{nP_c}{G_c A} \quad (15)$$

Substituting the P_{cel} calculated with (12)

$$\eta = \frac{nA_c}{A} \eta_c = F_R \eta_c \quad (16)$$

where F_R is the fill factor, relation between the total area occupied by the cells and area A of the module or the panel.

Experimentally, it was ascertained that the efficiency of a cell (or of a module, or a panel) at temperature T_c can be expressed as [6]

$$\eta = \eta_R [1 - \beta(T_c - T_R) + \gamma \log_{10} G_c] \quad (17)$$

with η_R the efficiency of the cell evaluated in reference conditions ($G_R = 1,000 \text{ W/m}^2$, $T_R = 298 \text{ K}$, air mass $m = 1$) and G irradiation expressed in kW. For silicon cells, it can normally be assumed that $\beta \cong 0.0045 \text{ }^\circ\text{C}^{-1}$ and $\gamma \cong 1.3$.

Often, the logarithmic term is neglected in calculations; therefore, (17) becomes

$$\eta = \eta_R [1 - \beta(T_c - T_a)] \quad (18)$$

The equation of instantaneous balance (12) can be written with reference to a panel:

$$P = AG_c \tau\alpha - AU_c(T_c - T_a) = \eta AG_c \quad (19)$$

with T_c average temperature of the panel, equal to the average temperature of the cells. Obtaining the cell temperature from (18) and substituting it in (19), the following expression is obtained for the efficiency:

$$\eta = \frac{\eta_R \left[1 - \beta(T_c - T_R) - \beta \frac{\tau\alpha G_c}{U_c} \right]}{1 - \eta_R \frac{\beta G_c}{U_c}} \quad (20)$$

which consents to the calculation of the instantaneous efficiency of the panel given the instantaneous values of the environmental temperature T_a and of the solar irradiation G_c . Often, for calculation simplicity, the denominator is assumed to be unitary. Given the known instantaneous efficiency of the cell evaluated with (20), the relation (19) permits the calculation of the instantaneous temperature of the cells.

Finally, in the energy performance calculations of a photovoltaic plant, it is useful to determine the average monthly efficiency, relation between the total energy produced and the total incident energy in the same time frame. Such an evaluation is obtained considering the average hourly values of the efficiency and irradiation according to the relation:

$$\bar{\eta} = \frac{\int_{\text{hour}} \eta G dt}{\int_{\text{hour}} G dt} = \frac{\sum \eta G \Delta t}{\sum G \Delta t} \quad (21)$$

with Δt time interval equal to 1 h.

The evaluation of the thermal power lost by the panel due to transmission towards the external environment requires the determination of the thermal exchange coefficient. A simple method is based on the knowledge of the nominal operative temperature of the cell Nominal Operative Cell Temperature (NOCT) [2]. This measurement represents the cell temperature, experimentally measured in its working position, in an open circuit (zero electrical power), in incident irradiation conditions equal to 800 W/m^2 , wind velocity of 1 m/s and environment temperature of $20 \text{ }^\circ\text{C}$. In such conditions, by applying (14), the following is obtained:

$$\frac{\tau\alpha}{U_c} = \frac{\text{NOCT} - 20}{800} \quad (22)$$

In this way, it is possible to determine the thermal exchange coefficient for the considered reference conditions, given the produced $\tau\alpha$ by the cell covering system. The NOCT value is usually provided by the constructors and assumes values which vary between $40\text{--}45 \text{ }^\circ\text{C}$.

5.1 Photovoltaic Cell Types and Plant Components

One of the main limits of photovoltaic technology is linked to the high costs and to the limited efficiency of conversion of solar radiation into electrical energy. The research of materials which that ensure high electrical efficiencies and contained costs has always been developed according to different technological approaches [7]. Monocrystalline silicon ensures efficiency which varies little over time and necessitates high costs for the preparation of the monocrystalline. In order to reduce production costs, the photovoltaic industry uses cells with polycrystalline silicon as an alternative, in which the crystals are still aggregated yet with different

forms and orientations. The nominal efficiency of silicon cells available on the market varies between 14 and 17.5 %.

Thin-film cells are formed by thin layers of semiconductor materials applied on a solid support. The use of a thin film notably reduces the quantity of semiconductor material necessary in the cell, compared to crystalline silicon wafers, and consequently even the production costs are reduced. The most commonly used materials in these types of cells are amorphous silicon (a-Si), gallium arsenide (GaAs), cadmium telluride (CdTe) and copper indium diselenide (CuInSe₂). Overall, the efficiency of thin-film cells is lower than those in crystalline silicon. Those currently available on the market present efficiency values which vary between 3.5 and 10.5 % with a lesser dependence on cell temperature due to the lower value of the temperature coefficient β which appears in the expression of the cell efficiency.

In third-generation photovoltaic cells, the most widely used materials for the creation of organic solar cells are molecular and polymeric semiconductors, such as fullerene (C₆₀) and all its derivatives [8]. These materials are already widely used in the electronic industry, and interest lies in the simplicity and economy of the production processes. In the majority of cases, the efficiency obtained is relatively limited, currently less than 5 %, and data inherent to cell stability and energy return time are not yet available.

Given the scant power generated by a single module, it is indispensable to connect the modules in series and in parallel in order to obtain the desired current and tension values. A group of modules connected in a rigid structure is called a panel. A group of panels connected in a series in such a way as to supply nominal tension of the plant is called a string. All the panels which are connected together form the electrical energy generator, or photovoltaic field.

In order to compensate for the precariousness of the solar source, compared to the continuous requests of an electrical load, the plant can be connected in parallel to the electrical grid, or equipped with storage batteries. The maximum power tracking system “maximum power point tracker” (MPPT) allows the photovoltaic field to always operate with optimal tension and current values.

If it is necessary to have electrical energy in the form of monophase or triphase current (the modules produce continuous current), static converters, called inverters, are used. Modern MPPT are integrated with inverter devices and also carry out other functions such as the protection of loads; they realise a parallel connection between the different strings and have the function of acquiring functioning data.

5.2 Dimensioning of Photovoltaic Generators

The planning of photovoltaic plants is executed with simplified methods using different methods according to whether one is dealing with plants which are directly connected to the electrical grid (so-called grid connected, which are

widespread) or plants which are for isolated users who use a battery system to store electrical energy (stand-alone). In the latter case, as well as planning the generator, it is also necessary to design the storage system to limit, as much as possible, the electrical energy produced and not consumed which needs to be dissipated in the case of battery saturation.

Grid-connected plants favourably benefit from being connected to the national grid, which can be considered as the ideal storage system to which it is to return the excess electrical energy produced.

The planning of a photovoltaic generator can be made in terms of power, or, and in the majority of cases, according to energetic criteria using the annual energy requirement as the reference parameter. The sizing of the plant requires evaluations of an economic nature, considering any eventual incentive campaigns.

There are two commonly used simplified energetic methods: the Siegel et al. method [9] and the Clark et al. method [10]. The two methods are applicable both for verification and for the basic planning of the plants. The first is valid in the case that the electrical energy produced is contemporaneously absorbed by the load, assumed to be constant. This hypothesis is true in the case of grid-connected plants, in which the eventual excess electrical power produced, compared to that absorbed by the load, is supplied to the grid. The method estimates the average monthly daily efficiency of the photovoltaic field from the average monthly daily irradiation values.

The second method considers the variable hourly profiles of the electrical load and uses the hourly irradiation values in average monthly days. In the following paragraph, a simplified model for the evaluation of the annual energy obtainable per peak kWh in the case of plants which are connected directly to the grid is shown.

5.3 Simplified Procedure for the Evaluation of Electrical Energy Producible in Buildings

In buildings which are subject to important renovation works, and also in new buildings, the evaluation of annually produced energy by photovoltaic panels can be obtained by a simplified procedure. This simplified procedure is sufficiently accurate and uses the energy values determined considering a reference placement of the panels and corrective factors to take into account their eventual different orientation and tilt [5]. The procedure lends itself to being applied in an efficient manner to buildings in the case in which the pitched roof surfaces are used for collection, which usually are differently oriented and tilted.

The calculation method uses the annual electrical power producible (kWh/kWp), determined considering a south-facing surface ($a_w = 0^\circ$) and inclined at an angle $\beta = 30^\circ$, with a collection area equal to that required for a nominal peak power of 1 kW. The described collection surface can be considered as a reference for latitudes between 35°N and 45°N .

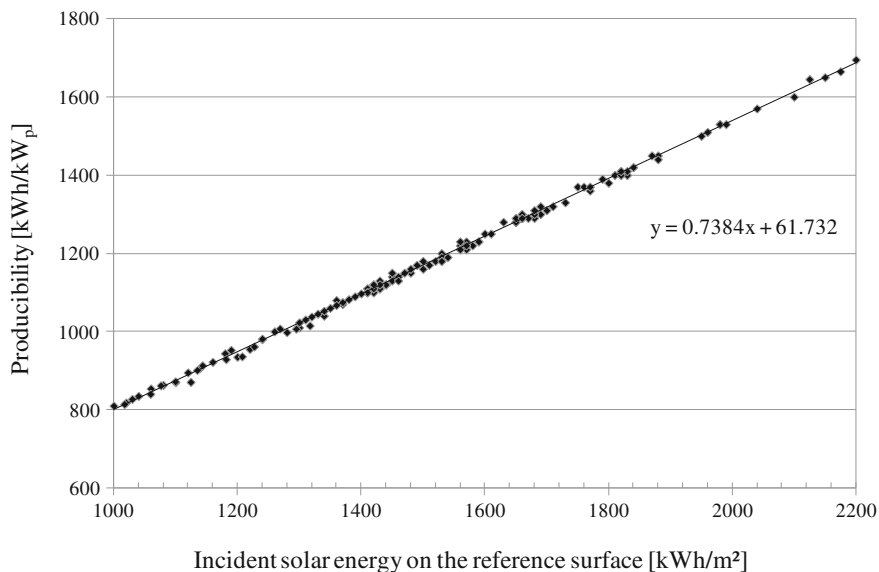


Fig. 5 Producibile electrical energy on the reference plane ($a_w = 0^\circ$, $\beta = 30^\circ$) varying the annual solar radiation on the horizontal plane

The annual electrical energy (kWh/kWp) which can be produced is reported in Fig. 5, for mono- or polycrystalline cells, as a function of the solar energy available on the horizontal plane (kWh/m^2). The radiation data considered are those relative to the European climatic conditions. The energy which can be produced varies between 1,050 and 1,600 kWh/kWp and can be considered, with a good approximation, a linear function of the solar radiation available on the horizontal plane.

In order to evaluate the electrical producibility varying the arrangement of the collection surface, the corrective factor FC, defined as the relation between the electrical energy produced on the considered surface (a_w, β) and the corresponding energy on the reference surface, is used:

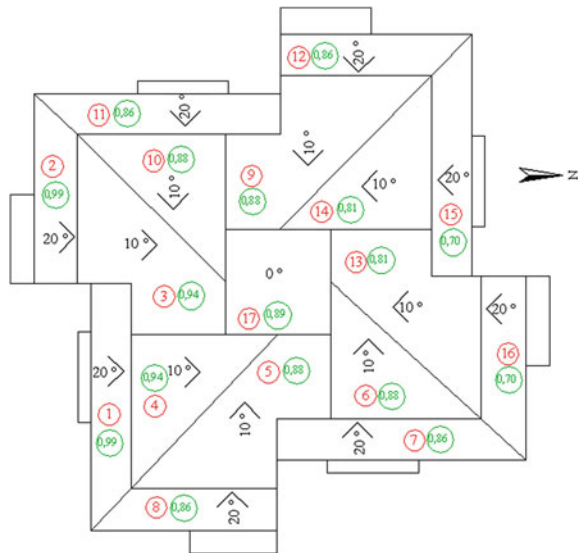
$$FC = \frac{E_{el}(a_w, \beta)}{E_{el}(a_w = 0^\circ, \beta = 30^\circ)} \quad (23)$$

The FC factor values are provided by Table 5 and are valid for values of angle β which are variable between 0° and 90° and an azimuth between 0° and 180° , in such a way as to also include the photovoltaic field layout on vertical walls. The FC values can be held to be valid for latitudes between 35°N and 45°N with variances which do not exceed 3 %. Starting from the reference energy, the FC factor allows for the determination of the electrical energy produced on a surface which is oriented and inclined.

Table 5 FC corrective factor values of the reference producibility varying the grade angle β and the azimuth a_w of the collection surface

β (°) \rightarrow a_w (°)↓	0	10	20	30	40	60	90
180	0.88	0.80	0.70	0.60	0.50	0.32	0.15
157.5	0.88	0.81	0.71	0.62	0.53	0.36	0.19
135	0.88	0.82	0.75	0.67	0.60	0.46	0.27
112.5	0.88	0.84	0.80	0.75	0.70	0.58	0.38
90	0.88	0.88	0.86	0.83	0.80	0.70	0.48
67.5	0.88	0.91	0.91	0.90	0.88	0.80	0.57
45	0.88	0.92	0.95	0.96	0.95	0.87	0.62
22.5	0.88	0.94	0.98	0.99	0.98	0.91	0.65
0	0.88	0.95	0.98	1.00	1.00	0.92	0.64

Fig. 6 Example of the roof of an existing building object of a photovoltaic installation



The procedure applied to different surfaces of the covering of a pitched roof allows for a classification of their production of electrical energy.

Example 2 Figure 6 represents a plan of the roof of building situated in Rome. The reference number, tilt angle β , azimuth a_w , and the FC corrective factor of the electrical producibility using the values from Table 5 are written on each slope. In the hypothesis that only 50 % of the slope surfaces can be used for collection, determining for a plant with peak power of 5 kW, the production of electrical energy obtainable from the different surfaces and the layout of the photovoltaic field ensures the maximum production of energy. *Data:* annual solar radiation available on horizontal plane 1,600 kWh/m²; necessary surface area of panels for a peak power of 1 kW equal to 8 m².

Table 6 Calculation results

Slope N.	a_w (°)	β (°)	Area (m ²)	Effective area (m ²)	f_c	Producibility (kWh/kW _p)	Installable power (kW)	Energy produced (kWh/year)	
S	1	0	20	36.5	18	0.99	1,231	2.2	2,707
	2	0	20	27.7	14	0.99	1,231	1.7	2,092
	3	0	10	56.9	28	0.94	1,168	3.5	4,089
	4	0	10	40.5	20	0.94	1,168	2.5	2,921
HZ	17	–	0	39.1	20	0.89	1,106	2.4	2,655
E	5	90	10	52.1	26	0.88	1,094	3.2	3,500
	6	90	10	36.6	18	0.88	1,094	2.2	2,406
W	9	90	10	58.4	29	0.88	1,094	3.6	3,938
	10	90	10	39.1	20	0.88	1,094	2.4	2,625
E	7	90	20	36.9	18	0.86	1,069	2.3	2,459
	8	90	20	29.4	15	0.86	1,069	1.8	1,924
W	11	90	20	37.3	19	0.86	1,069	2.3	2,459
	12	90	20	29.4	15	0.86	1,069	1.8	1,924
N	13	180	10	56	28	0.81	1,007	3.5	3,524
	14	180	10	42	21	0.81	1,007	2.6	2,618
	15	180	20	36.6	18	0.70	870	2.2	1,914
	16	180	20	30.8	15	0.70	870	1.9	1,653

From the graphic in Fig. 5, for an availability of energy of 1,600 kWh/m², the reference producibility is equal to 1,243 kWh/kW_p. Using the available slope surfaces, the results obtainable in the production of electrical energy are summarised in Table 6. For each slope, the following data are reported: azimuth a_w , grade β , corrective factor FC, available surface area, surface area that can be used, producibility, installable power and energy produced.

The greatest production of electrical energy is obtained using slope numbers 1, 2 and 3. For a peak power of 5 kW, it is necessary to install $5 \cdot 8 = 40$ m² panels.

Considering that the usable surface for each slope is as follows:

Panel surface on slope n. 1:	18 m ²
Panel surface on slope n. n. 2:	14 m ²
Panel surface on slope n. n. 3:	$40 - 18 - 14 = 8$ m ²

Therefore, the total production is $2,707 + 2,092 + \frac{8}{28} \cdot 4,089 = 5,967$ kWh/year

6 Direct Gain Passive Solar Systems

A glazed surface and the relative belonging environment form a direct gain passive system and represent the simplest and most economic system to use solar energy. In such a system, the solar radiation entering the glazed surfaces is in part absorbed by the environment walls, which have the function of thermal absorber and storage, and in part exits through the same glazed surface. The thermal level of the energy stored in the walls of a cavity depends on their dynamic properties, which determine the fraction of energy absorbed which is ceded to the indoor air. Such contributions give rise to a reduction in the winter thermal requirements and to an increase in the requirement during summer.

Another shell component which is easily realisable in buildings is the sunspace, which allows for architectural solutions which are of interest from an energy viewpoint. The control of entering radiation through the shell, by means of screens, and the possibility of using airflow rates for ventilation of the sunspace allows for the reduction in the energy requirement of the adjacent environment and, at the same time, creates acceptable thermal conditions within the sunspace.

6.1 Solar Gain Through Windows

The solar power entering in an environment through the glazed surface unit is given by the relation:

$$G_e = I_{b0}R_b\tau_b + I_{d0}R_d\tau_d + (I_{b0} + I_{d0})R_r\tau_g \quad (24)$$

with I_{b0} and I_{d0} direct and diffuse radiation on the horizontal plane; R_b , R_d and R_r , respectively, inclination factor of direct, diffuse and reflected radiation and τ_b , τ_d and τ_g transmission coefficient of the glazed system of the direct, diffuse and reflected radiation [2].

If the instantaneous transmission coefficient of global radiation τ is introduced, the former can be expressed in the form of

$$G_e = G\tau \quad (25)$$

with G incident solar power on the external surface of the glass and τ given by the relation:

$$\tau = \frac{I_{b0}R_b\tau_b + I_{d0}R_d\tau_d + (I_{b0} + I_{d0})R_r\tau_g}{I_{b0}R_b + I_{d0}R_d + (I_{b0} + I_{d0})R_r} \quad (26)$$

The daily average monthly energy entering the glazed surface unit can be evaluated by considering the daily average monthly values of the quantities that appear in the relation (24):

$$\bar{E}_e = \bar{E}R_b\bar{\tau}_b + \bar{D}R_d\tau_d + (\bar{B} + \bar{D})R_r\tau_g \quad (27)$$

Table 7 Average monthly transmission coefficient for simple clear glass (thickness = 4 mm) varying exposure

Month	Jan	Feb	Mar	Apr	May	Jun	Jul	Aug	Sep	Oct	Nov	Dec
<i>South</i>												
Milan	0.799	0.785	0.750	0.700	0.656	0.637	0.646	0.683	0.731	0.776	0.796	0.802
Rome	0.795	0.779	0.740	0.683	0.635	0.617	0.626	0.664	0.718	0.769	0.792	0.799
Messina	0.791	0.772	0.728	0.664	0.614	0.602	0.607	0.643	0.704	0.761	0.787	0.795
<i>East/west</i>												
Milan	0.706	0.731	0.747	0.753	0.754	0.753	0.753	0.753	0.749	0.736	0.713	0.697
Rome	0.714	0.734	0.748	0.753	0.753	0.751	0.752	0.752	0.750	0.739	0.720	0.706
Messina	0.720	0.737	0.748	0.752	0.752	0.750	0.751	0.752	0.750	0.740	0.724	0.713
<i>North</i>												
Milan	0.730	0.730	0.730	0.712	0.674	0.669	0.672	0.696	0.730	0.730	0.730	0.730
Rome	0.730	0.730	0.730	0.711	0.670	0.664	0.667	0.695	0.730	0.730	0.730	0.730
Messina	0.730	0.730	0.730	0.710	0.666	0.658	0.662	0.692	0.730	0.730	0.730	0.730

The calculation procedure of the average monthly direct radiation inclination factor \bar{R}_b is reported in [2]. Alternatively, in (27), the relation can be reused:

$$\bar{E}_e = \bar{E}_i \bar{\tau} \quad (28)$$

with E_i daily average monthly energy incident on the external glazed surface and $\bar{\tau}$ transmission coefficient of the daily average monthly global radiation which can be evaluated with the relation:

$$\tau = \frac{\bar{E}\bar{R}_b\bar{\tau}_b + \bar{D}R_d\tau_d + (\bar{B} + \bar{D})R_r\tau_g}{\bar{E}\bar{R}_b + \bar{D}R_d + (\bar{B} + \bar{D})R_r} \quad (29)$$

In Tables 7 and 8, the $\bar{\tau}$ values for simple and double clear glass in clear sky conditions are reported for three Italian localities, Milan, Rome and Messina. Comparable results can be obtained for Bordeaux, Barcelona and Athens, respectively [11].

The solar radiation which is transmitted through glazed surfaces undergoes numerous reflections within the environment. Upon each reflection, the radiation attenuates due to the absorption caused by the walls, and the radiation which falls from the indoor space on the same glazed surface is, in part, dispersed externally.

The effective absorption coefficient of the environment α_{cav} is the ratio between the absorbed solar power and the entering solar power:

$$\alpha_{cav} = \frac{Q_{ass}}{A_f G_e} \quad (30)$$

The power absorbed by the space, or net solar gain, can be calculated, taking into account (31), with the relation:

$$Q_{ass} = A_f \alpha_{cav} \left[I_{b0} R_b \tau_{b/i} + I_{d0} F_{r-s} \tau_d + (I_{b0} + I_{d0}) \frac{\rho}{2} \tau_g \right] \quad (31)$$

Table 8 Average monthly transmission coefficient for double clear glass (4/12/4 mm) varying exposure

Month	Jan	Feb	Mar	Apr	May	Jun	Jul	Aug	Sep	Oct	Nov	Dec
<i>South</i>												
Milan	0.653	0.636	0.596	0.541	0.492	0.471	0.481	0.522	0.575	0.625	0.649	0.656
Rome	0.648	0.629	0.584	0.522	0.469	0.452	0.460	0.501	0.561	0.617	0.644	0.652
Messina	0.643	0.621	0.570	0.500	0.447	0.438	0.442	0.478	0.544	0.608	0.639	0.648
<i>East/west</i>												
Milan	0.549	0.576	0.594	0.601	0.602	0.600	0.600	0.601	0.597	0.582	0.557	0.539
Rome	0.557	0.580	0.595	0.601	0.600	0.599	0.599	0.600	0.597	0.585	0.564	0.549
Messina	0.564	0.583	0.596	0.600	0.599	0.598	0.598	0.599	0.597	0.587	0.569	0.557
<i>North</i>												
Milan	0.572	0.572	0.572	0.556	0.515	0.509	0.512	0.539	0.572	0.572	0.572	0.572
Rome	0.572	0.572	0.572	0.555	0.512	0.504	0.508	0.538	0.572	0.572	0.572	0.572
Messina	0.572	0.572	0.572	0.554	0.507	0.498	0.503	0.536	0.572	0.572	0.572	0.572

- f_i is a shading factor due to the presence of external obstacles which intercept direct radiation, or of special overhangs which, during summer, reduce the solar gain. These effects are evaluated reducing the windowed surface A_f by means of the coefficient f_i ;
- F_{r-s} is the view factor between the window and the sky (for a glazed surface which presents a horizontal overhang placed above it, the view factor values F_{r-s} are reported in Ref. [12]);
- F_c is a control function, which is equal to one when the glazed surface is not screened and equal to zero when an opaque screen for solar radiation is present; it is less than one when incident radiation is partially screened.

The daily average monthly solar energy absorbed by a space, due to the presence of a glazed surface, can be calculated considering the daily average monthly values of the quantities present in the relation (32):

$$\bar{E}_{ass} = A_f \bar{\alpha}_{cav} \left[\bar{B} \bar{R}_b \bar{\tau}_b \bar{f}_i + \bar{D} F_{r-s} \tau_d + (\bar{B} + \bar{D}) \frac{\rho}{2} \tau_g \right] \bar{F}_c \tag{32}$$

with \bar{f}_i average monthly value of the shade factor [12] and \bar{F}_c average value weighted on the radiation of the control function F_c .

6.2 Estimation of the Daily Average Monthly Absorption Coefficient of the Environments

The solar radiation which penetrates an environment through a glazed surface in part is direct radiation and in part is diffuse radiation. A simplification which is usually adopted is that of supposing solar radiation which emerges from the glazed surface, within the environment, as diffuse radiation; in this way, the directional

aspects of the entering radiation are not considered. In such conditions, with reference to environments of a parallelepiped shape, with different ratios of the sides in plan and with one or more differently oriented glazed surfaces, the daily average monthly absorption coefficient of the environment α_{cav} , can be made to depend [13]

- on the average absorption coefficient of the opaque surfaces of the environment:

$$\alpha_m = \frac{\sum_i \alpha_i A_i}{\sum_i A_i} \quad (33)$$

with α_i absorption coefficient in the solar band of the surfaces A_i ,

- on the glazed fraction of the environment, ratio between the glazed area and the opaque area of the cavity

$$\Psi = \frac{\sum_j A_{v,j}}{\sum_i A_i} \quad (34)$$

- on the optical properties of the glazed system, defined through the transmission coefficient of diffuse solar radiation τ_d .

The functional bond is expressed by the relation:

$$\alpha_{\text{cav}} = 1 - a \exp \left[-b \left(\frac{\alpha_m}{\Psi} \right)^2 \right] \quad (35)$$

with coefficients a , b and c ; quadratic functions of the transmission coefficient of diffuse radiation of the glazed system:

$$\begin{aligned} a &= 3.500 - 5.453\tau_d + 4.516\tau_d^2 \\ b &= 3.700 - 5.388\tau_d + 3.462\tau_d^2 \\ c &= 0.124 + 0.545\tau_d - 0.355\tau_d^2 \end{aligned} \quad (36)$$

The correlation (36) is valid for α_m variable between 0.20 and 0.80; Ψ inclusive between 0.025 and 0.60 and for glazed systems formed in the following manner: single clear 4-mm glass; double glazing with two 4-mm glass panes and a 16-mm air gap; and double glazing with three 2.5-mm glass panes and 12-mm air gaps. For such glazed systems, the corresponding values of the diffuse radiation transmission coefficient τ_d are, respectively, equal to 0.79, 0.59 and 0.51.

The values of the daily average monthly absorption coefficient evaluated with the previous relations, for environments with different value of the ratio between the effective absorption area and the glazed area $\alpha_m \Psi$, are reported in Table 9.

Table 9 Values of the effective absorption coefficient of environments with different glazed systems varying the parameter α_m/Ψ

α_m/Ψ	Single glass	Double glazing	Triple glazing
	α_{cav}	α_{cav}	α_{cav}
0.33	0.29	0.42	0.48
0.60	0.47	0.58	0.62
1.33	0.67	0.74	0.77
2.10	0.76	0.81	0.83
2.40	0.78	0.83	0.85
3.00	0.81	0.85	0.87
3.87	0.85	0.88	0.89
4.90	0.87	0.90	0.91
5.80	0.89	0.92	0.93
6.20	0.90	0.92	0.93
7.50	0.91	0.93	0.94
9.00	0.93	0.94	0.95
10.50	0.94	0.95	0.96
12.40	0.95	0.96	0.96
18.60	0.97	0.97	0.98
24.80	0.98	0.98	0.98

6.3 A Complete Model for the Calculation of Solar Gains in Windowed Environments

If one considers an environment with one or more glazed surfaces, the daily average monthly solar gain through the glazed surfaces, following the calculation scheme deriving from the EN 410 (2011) Standard [29], can be evaluated with the relation:

$$Q_{sol} = \sum_k F_{sh,k} F_{sh,sl,k} (1 - F_{F,k}) A_{w,k} G_k F_{w,k} [\tau_{b,n} \alpha_{cav} + q_i + \tau_{b,n} (1 - \alpha_{cav}) q_e]_k \Delta t \tag{37}$$

with $F_{sh,k}$ and $F_{sh,gl,k}$ which are, respectively, the reduction factors for shading produced by external elements and due to the presence of mobile screens, for the k th surface; $F_{F,k}$ factor of the area relative to the frame; $A_{w,k}$ area of the window opening; G_k solar radiation; $F_{w,k}$ average corrective factor on the radiation incidence angles; $\tau_{b,n}$ coefficient of direct solar transmission due to normal incidence; q_i “internal” secondary radiative–convective thermal exchange inwards; q_e “external” secondary radiative–convective thermal exchange outwards; and Δt time interval.

In relation (37), in the square brackets, the first term $\tau_{b,n} \alpha_{cav}$ represents the direct optical fraction of solar radiation absorbed by the environment; the second term q_i the secondary direct fraction, produced by the absorption of the incident solar radiation from outside and the third term, the secondary indirect fraction,

Table 10 Optical and thermal parameters of the considered glazed systems

Glazed system	$g_{gl,n}$	$\tau_{b,n}$	τ_d	$\alpha_{b,n1}$	$\alpha_{b,n2}$	$\alpha_{b,n3}$	A_{12} (W/m ² K)	A_{23} (W/m ² K)	q_i	q_e
Single	0.857	0.830	0.749	0.095	–	–	–	–	0.027	0.068
Double	0.761	0.693	0.590	0.101	0.080	–	5.03	–	0.068	0.113
Triple	0.705	0.624	0.512	0.084	0.069	0.055	5.46	5.46	0.081	0.127

generated by the fraction reflected by the indoor surfaces $\tau_{b,n}(1 - \alpha_{cav})$ exiting the environment through the glazed surfaces. In the case of black cavity ($\alpha_{cav} = 1$), the term linked to the secondary indirect gain is annulled.

While the effective absorption coefficient α_{cav} characterises the environment with reference to the energy entering through the glazed surface, the parameter

$$g_{n,eff} = \tau_{b,n}\alpha_{cav} + q_i + \tau_{b,n}(1 - \alpha_{cav})q_e \quad (38)$$

characterises the absorption of solar radiation in the system formed by the environment and by the glazed surface, with reference to the incident solar energy on the external surface of the glass. This represents the effective solar gain coefficient of the environment and is a function of the optical and thermal properties of the glazed surface and of the optic properties and the geometrical properties of the environment.

The use of the relation (38) requires the determination of parameters $\tau_{b,n}$, q_i and q_e which are obtainable from the EN ISO 13790 (2008) Standard [30]. Given the known coefficient of total solar gain for normal incidence of the glazed system, the relation

$$g_{gl,n} = \tau_{b,n} + q_i \quad (39)$$

allows the calculation of the transmission factor $\tau_{b,n}$, given that the secondary thermal exchange expressions q_i for single, double and triple glass are known. The “external” secondary thermal exchange factor q_e can be calculated, for example, for a transparent system with three panes, with the relation:

$$q_e + q_i = \alpha_{b,n1} + \alpha_{b,n2} + \alpha_{b,n3} \quad (40)$$

with $\alpha_{b,n1}$, $\alpha_{b,n2}$ and $\alpha_{b,n3}$ direct absorption factors for normal incidence angle, respectively, for the first, second and third glass of the glazed system [30].

Table 10 provides, for the glazed systems defined in the preceding paragraph, the optical parameters for normal incidence and thermal ones which intervene in the calculation: the total solar gain coefficient $g_{gl,n}$, direct $\tau_{b,n}$ and diffuse τ_d solar radiation transmission, the direct absorption factors of the glazed sheets $\alpha_{b,n}$, the thermal conductance between the glass sheets A , and the “internal” q_i and “external” q_e secondary thermal exchange factors.

With an increase in the number of panes that form the glazed system, the optical parameters $g_{gl,n}$, $\tau_{b,n}$ and τ_d reduce, while the internal q_i and external q_e thermal exchange factors increase.

Table 11 provides the optical and thermal properties of double glazing

$\tau_d = 0.59$	$g_{gl,n} = 0.761$	$\tau_{b,n} = 0.693$	$q_i = 0.068$	$q_e = 0.113$
-----------------	--------------------	----------------------	---------------	---------------

Example 3 Consider an environment with a dimension, on plans, of 6×6 m and a height of 3 m, with three dispersant vertical walls, facing south, east and west, and the remaining opaque vertical and horizontal bordering air-conditioned environments. In the hypothesis that the external vertical walls are in part opaque, and in part glazed, in different relations, determine the effective solar gain coefficient of the environment $g_{n,eff}$ and the percentage weight of the three fractions of the solar gain. The opaque surfaces are clear with absorption coefficient in the solar band $\alpha_i = 0.30$. The optical and thermal parameters of the considered glazed systems are reported in Table 11.

For an environment with a glazed surface of 18 m^2 , one obtains

$$\alpha_m = \alpha_i = 0.30$$

$$\psi = \frac{18}{126} = 0.1429$$

The coefficients of the correlations calculated with (36) are as follows:

$a = 1.855$	$b = 1.726$	$c = 0.322$
-------------	-------------	-------------

The absorption coefficient of the cavity evaluated with (35) is

$$\alpha_{cav} = 0.793$$

The solar gain fractions are determined as follows:

$$\tau_{b,n}\alpha_{cav} = 0.693 \cdot 0.793 = 0.549$$

$$q_i = 0.068$$

$$\tau_{b,n}(1 - \alpha_{cav})q_e = 0.693 \cdot (1 - 0.793) \cdot 0.113 = 0.016$$

Finally, the effective solar gain coefficient results as being equal to

$$g_{n,eff} = 0.549 + 0.068 + 0.016 = 0.633$$

The percentages corresponding to the three solar gain fractions are 86.7, 10.7 and 2.6 %.

The values, for the same environment and for the three considered glazed systems, which are assumed by the three gain fractions varying the glazed surface from 4.5 m^2 (one glazed surface on one wall) to 54 m^2 (three completely glazed vertical surfaces) are reported in Table 12.

Table 12 Solar gains for an environment with different fractions Ψ and for different glazed systems

Glazed system	A_T (m ²)	Ψ	α_{cav}	$\tau_{b,n} \alpha_{cav}$	q_i	$\tau_{b,n} (1 - \alpha_{cav}) q_e$	$g_{n,eff}$	$\frac{\tau_{b,n} \alpha_{cav}}{g_{n,eff}}$ (%)	$\frac{q_i}{g_{n,eff}}$ (%)	$\frac{\tau_{b,n} (1 - \alpha_{cav}) q_e}{g_{n,eff}}$ (%)
Single	4.5	0.0323	0.933	0.775	0.027	0.0038	0.805	96.2	3.4	0.5
	9	0.0667	0.862	0.716	0.027	0.0078	0.751	95.4	3.6	1.0
	13.5	0.1034	0.803	0.666	0.027	0.0111	0.704	94.6	3.8	1.6
	18	0.1429	0.751	0.623	0.027	0.0141	0.664	93.8	4.1	2.2
	22.5	0.1852	0.705	0.585	0.027	0.0167	0.628	93.0	4.3	2.8
	27	0.2308	0.662	0.550	0.027	0.0191	0.596	92.3	4.5	3.4
	40.5	0.3913	0.552	0.458	0.027	0.0253	0.510	89.8	5.3	5.4
	54	0.6000	0.456	0.378	0.027	0.0307	0.436	86.8	6.2	7.7
	4.5	0.0323	0.946	0.656	0.068	0.0042	0.728	90.1	9.3	0.6
	9	0.0667	0.887	0.615	0.068	0.0088	0.692	88.9	9.8	1.3
Double	13.5	0.1034	0.837	0.580	0.068	0.0128	0.661	87.8	10.3	1.9
	18	0.1429	0.793	0.549	0.068	0.0162	0.634	86.7	10.7	2.6
	22.5	0.1852	0.753	0.522	0.068	0.0193	0.609	85.7	11.2	3.2
	27	0.2308	0.717	0.497	0.068	0.0222	0.587	84.6	11.6	3.8
	40.5	0.3913	0.620	0.429	0.068	0.0298	0.527	81.5	12.9	5.6
	54	0.6000	0.534	0.370	0.068	0.0365	0.474	78.0	14.3	7.7
	4.5	0.0323	0.953	0.595	0.081	0.0037	0.679	87.5	11.9	0.6
	9	0.0667	0.901	0.562	0.081	0.0079	0.651	86.3	12.4	1.2
	13.5	0.1034	0.855	0.534	0.081	0.0115	0.626	85.2	12.9	1.8
	18	0.1429	0.815	0.509	0.081	0.0146	0.604	84.2	13.4	2.4
Triple	22.5	0.1852	0.779	0.486	0.081	0.0175	0.585	83.1	13.9	3.0
	27	0.2308	0.745	0.465	0.081	0.0202	0.566	82.1	14.3	3.6
	40.5	0.3913	0.655	0.409	0.081	0.0273	0.517	79.1	15.7	5.3
	54	0.6000	0.574	0.358	0.081	0.0337	0.473	75.7	17.1	7.1

7 Sunspaces

Sunspaces are passive solar systems which can be easily and profitably employed in the restructuring of buildings, due to the simplicity of their construction and the ease with which they can be integrated into the existing structure, for the reduction of the winter energy requirement. The energy performance in an environment adjacent to a sunspace is obtained by using the following: the direct solar gains, represented by the radiation which directly penetrates the environment through the glazed surfaces of the sunspace and of the glass dividing wall, and the indirect solar gains, produced by the fraction of solar energy which crosses the glazed shell of the sunspace and is absorbed by the opaque walls of the sunspace, with a successive transfer of energy to the air-conditioned environment, due to the presence of the sunspace in which the air temperature is generally higher than the external temperature.

The elements which determine sunspace performance are the following:

- orientation: it is preferable that the sunspace is in a south-facing position, thus ensuring greater solar gains during winter;
- the glazed system: by means of the optical and thermal properties of the glass surfaces and frame;
- the opaque elements: through the solar absorption coefficients and the thermal capacities;
- the shading systems: to reduce entering solar radiation and limit overheating of the air;
- ventilation: to remove energy from the sunspace and limit the air temperature and obtain acceptable conditions for the occupants.

During summer, sunspaces must be completely openable in order to efficiently contrast overheating of the air.

Sunspaces can be realised through different technological and formal solutions, in relation to the specific environmental, climatic and architectural contexts. It is possible to create a classification considering the sunspace elements and the wall to which it is attached, distinguishing between the following: an attached sunspace, which is developed in an external position in relation to the facade (Fig. 7); a glazed balcony, which is obtained by closing an embedded balcony (Fig. 8); and an embedded sunspace, which is in part developed inwards, and in part outwards (Fig. 9).

With regard to the extension of the solar radiation collection surface, it is possible to distinguish between entirely glazed systems and mixed glazed–opaque systems. Furthermore, the glazed system can be continuous, with a frame only on the upper and lower sides and not on the lateral sides, or with a frame which is visible on all sides.

Glazed surfaces are the most important components of sunspaces. The types of glass that are commonly used are as follows: simple clear glass, which presents optimal solar transparency qualities but poor thermal and acoustic insulation

Fig. 7 Attached sunspace in a single-family building and multi-family building

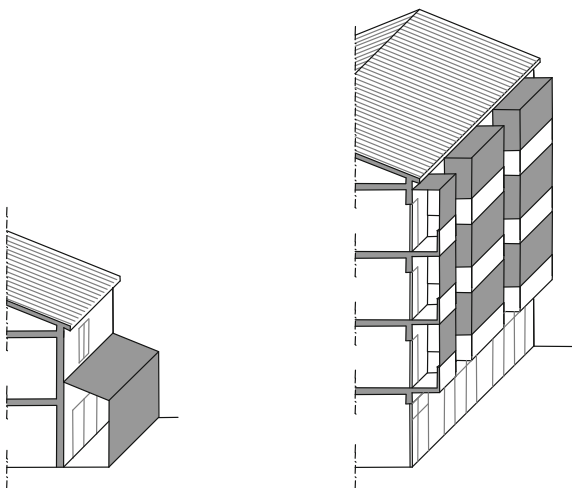


Fig. 8 Glazed balcony in a single-family and multi-family building

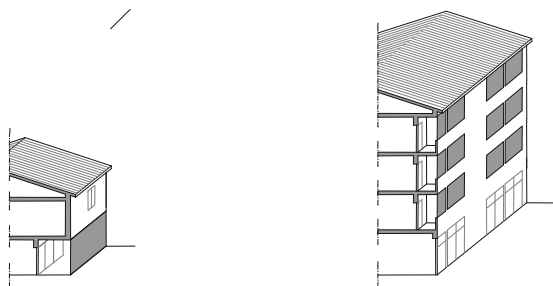
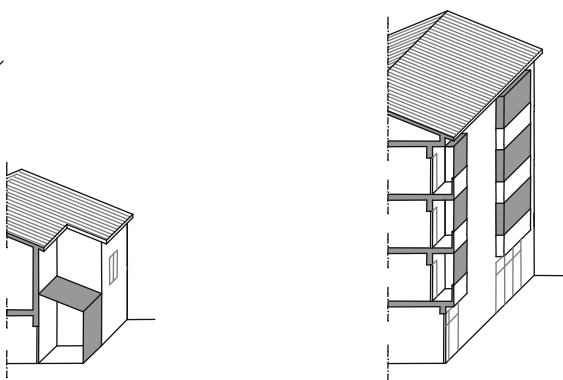


Fig. 9 Embedded sunspace in a single-family building and multi-family building



properties; double glazing, with reduced thermal transmittance values; low-emission glass, to further reduce thermal transmittance; and solar control glass, which favours the reflection of infrared solar radiation and the transmission of luminous solar radiation.

7.1 Thermal Balance of the Sunspace and Solar Gain

The solar radiation which is transmitted through the glazed shell of the sunspace is, in part, absorbed by the opaque and glass walls; in part it is lost towards the outside through the same glazed surfaces; in part it is transmitted to the adjacent environments by means of the separation elements.

The sunspace can be subject to flow rates; in such a case, it behaves as an open thermodynamic system which has exchanges of both energy and mass with the external environment and with the adjacent environments. The control of the mass and energy flows through the shell, obtained through appropriate ventilation and radiation shading strategies, allows for a reduction in the energy requirement of the adjacent building, and at the same time, creates acceptable thermal conditions within the sunspace.

The evaluation of solar gain in sunspaces requires the resolution of the optical field in the solar band, for the evaluation of the energy that is effectively absorbed by the walls, and the thermal field in the walls for the determination of the energy ceded to the internal air. For the latter evaluations, within the sunspace, it is necessary to determine the radiant field in the long infrared for the definition of the surrounding conditions.

With reference to the sunspace in Fig. 10, bordering with an adjacent environment and an underlying environment, both of which are air-conditioned, the equation of the thermal balance of the sunspace shell, formed by both opaque and glazed walls, with reference to a definite time interval, can be placed under the form:

$$Q_{as} + Q_{ai} + Q_{ae} + Q_w + Q_f = \Delta E_w + \Delta E_f \quad (41)$$

with Q_{as} energy absorbed by the sunspace walls; Q_{ai} energy that the internal surfaces exchange with the indoor air; Q_{ae} energy transferred externally; Q_w energy exchanged with the adjacent environment; Q_f energy exchanged with the underlying environment; ΔE_w variation of the internal energy of the wall and ΔE_f variation of the internal energy of the floor.

In Eq. (41), the variation of internal energy of the glazed walls was assumed to be negligible.

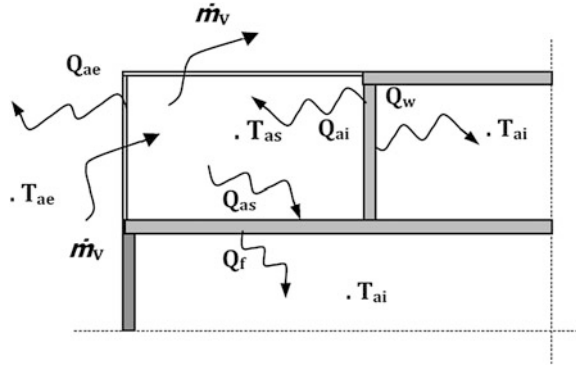
For the sunspace air volume, held to be a negligible thermal capacity, in the case that ventilation is realised with an external airflow rate, the balance equation is the following:

$$Q_{ai} = \dot{m}_v c_p (T_{as} - T_{ae}) \Delta t \quad (42)$$

with \dot{m}_v ventilation flow rate deriving from outside; T_{as} air temperature in the sunspace; T_{ae} external air temperature and c_p specific heat of the air.

In the absence of ventilation, $\dot{m}_v = 0$, and the total energy Q_{ai} exchanged by the air with the internal surfaces is annulled. Such a result is obtained by means of variable exchange configurations during diurnal hours in relation to the position of the sun, while during nocturnal hours, prevalently, the sunspace air receives energy from the opaque walls and cedes energy to the glazed walls.

Fig. 10 Thermal exchanges between the sunspace and the adjacent environments



The energy transmitted through the sunspace shell is obtained by the radiation transmission coefficient τ_e , ratio between the transmitted energy Q_{tr} and the incident energy Q_i :

$$\tau_e = \frac{Q_{tr}}{Q_i} \quad (43)$$

The energy absorbed is evaluated with the effective absorption coefficient of the sunspace α_s , ratio between the energy absorbed $Q_{as,s}$ and that transmitted Q_{tr} [14]:

$$\alpha_s = \frac{Q_{as,s}}{Q_{tr}} \quad (44)$$

The solar gains in the sunspace can be calculated by the utilisation factor, defined by the relation

$$\eta_u = \frac{Q_{ai}^+}{Q_{as,s}} \quad (45)$$

with $Q_{as,s}$ absorbed energy and Q_{ai}^+ energy transferred by convention to the internal air, to be evaluated with the relation

$$Q_{ai}^+ = \sum S_i h_{c,i} (T_i - T_{as})^+ \Delta t \quad (46)$$

With T_i internal surface temperature of the surfaces S_i and $h_{c,i}$ convective thermal exchange coefficients. The sign + indicates that in the summation, only the positive contributions are calculated. In absence of ventilation, the energy received from the air Q_{ai}^+ is ceded prevalently to the outside. In the presence of ventilation, the net energy received for convection from the air Q_{ai} is removed by the airflow rate, as shown by the Eq. (42). In such a case, the utilisation factor imputable to ventilation $\eta_{u,v}$ is calculated as the ratio between the energy removed by the ventilation flow rate Q_{ai} and the energy absorbed $Q_{as,s}$ [15]:

$$\eta_{u,v} = \frac{Q_{ai}}{Q_{as,s}} \quad (47)$$

In order to reduce the energy requirement of the adjacent environments, the important issue is the energy transferred at a temperature of more than 20 °C, or rather the quantity

$$Q_{ai,u}^+ = \dot{m}_v c_p (T_{as} - 20)^+ \Delta t \quad (48)$$

in such a case the effective utilisation factor $\eta_{u,v}^{\text{eff}}$ is given by the ratio between $Q_{ai,u}^+$ and the absorbed energy $Q_{as,s}$

$$\eta_{u,v}^{\text{eff}} = \frac{\dot{m}_v c_p (T_{as} - 20)^+ \Delta t}{Q_{as,s}} \quad (49)$$

Lastly, with regard to the thermal gains through the opaque walls, obtained by the adjacent environments, since the thermal flow on the wall can change directions, it is necessary to consider the relations $Q_w^+/Q_{as,s}$ and $Q_f^+/Q_{as,s}$, respectively, for the wall and the floor, with

$$Q_w^+ = S_w h_{c,w} (T_{s,w} - T_{ai})^+ \Delta t \quad (50)$$

$$Q_f^+ = S_f h_{c,f} (T_{s,f} - T_{ai})^+ \Delta t \quad (51)$$

with $h_{c,w}$ and $h_{c,f}$ convective coefficients of the wall and of the floor with the indoor air.

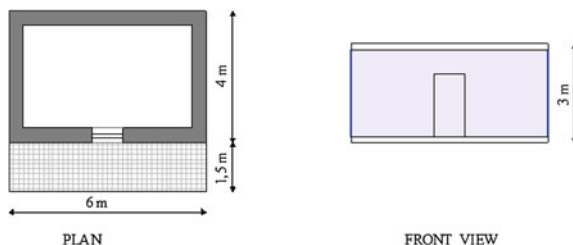
For the considered geometry, the previous relations allow for the determination of solar gains in the sunspace and in the adjacent environments, through the opaque elements and the ventilation flow rate. Such evaluations can be carried out on an hourly, daily and monthly basis.

7.2 Improvement in the Energy Performance of an Environment Adjacent to a Glazed Balcony

The optical and energy behaviour of a windowed environment is compared with that of the same environment equipped with a sunspace at the front. A total glazed sunspace was considered (Fig. 11) with different exposure (south, east/west) and situated in localities which are climatically different, Cosenza ($L = 39^\circ 18'$, Southern Italy) characterised by Mediterranean climate and Milan ($L = 45^\circ 27'$, Northern Italy) with continental climate. Similar climatic conditions, latitude, yearly solar irradiation and average monthly temperatures, are registered for Athens and Valencia in the Mediterranean area and for Belgrade and Bordeaux with continental climate.

The environment has a surface area of 24 m² and has a balcony in front of it, which is 6 m in length and 1.5 m in width. The closure of the balcony, by means of glazed elements, gives a sunspace with a volume equal to 27 m³. The adjacent environment presents two dispersive external walls, with a thermal transmittance

Fig. 11 Sunspace geometry—considered environment



of $0.95 \text{ W/m}^2 \text{ K}$ and a thermal capacity of $218 \text{ kJ/m}^2 \text{ K}$, while the remaining walls border with heated environments. The combinations considered in the optical analysis are differentiated for the solar absorption coefficient of the floor α_f and of the walls α_w : $\alpha_f = \alpha_w = 0.2$ and $\alpha_f = \alpha_w = 0.5$, and furthermore $\alpha_f = 0.5$ and $\alpha_w = 0.2$ both for the sunspace and the adjacent environment. The glazed system is clear double glazing 4–12–4 mm with a thermal transmittance of $U = 2.88 \text{ W/m}^2 \text{ K}$ and total solar transmission coefficient $g = 0.75$. The environment is separated by the environment by means of a wall with a glazed fraction which is variable between 20 and 100 %.

The presence of the sunspace gives rise to greater incident energy on the external glazed shell, to a reduction in the direct solar gain through the windowed surface of the environment and to a reduction in the thermal losses outwards, through the dividing wall, due to the increase in the air temperature in the sunspace compared to the external temperature.

The effective average monthly coefficient of the environment in absence and in presence of the sunspace, and the effective absorption coefficient of the sunspace are reported in Figs 12 and 13, varying the optical properties of the environments and of the glazed fraction of the dividing wall.

The presence of the sunspace leads to a decrease in the absorption coefficient of the environment α_{as} , due to the reduction in the absorbed energy and, to a greater extent, due to the effect of the increase in the energy entering the external glazed surface. Moreover, the presence of the sunspace introduces a significant monthly variability during winter months on decreasing the glazed fraction of the environment.

If the sunspace is facing east, in the same conditions, no significant variation of the absorption coefficients is recorded compared to southern exposure.

Figures 14 and 15 with reference to the heating period (15/11–31/3) show the energy absorbed by the environment, by the environment with the sunspace and by the sunspace, varying the glazed fraction of the dividing wall, for the three optical combinations considered.

Both for southern and eastern exposure, the reduction in energy absorbed by the environment due to the effect of the sunspace is little influenced by the glazed fraction f and increases with the absorption coefficient of the walls. For reflective environments, the reduction is around 30 %, and for more absorbent environments, the reduction is 35 %. With regard to the sunspace, the absorbed energy increases

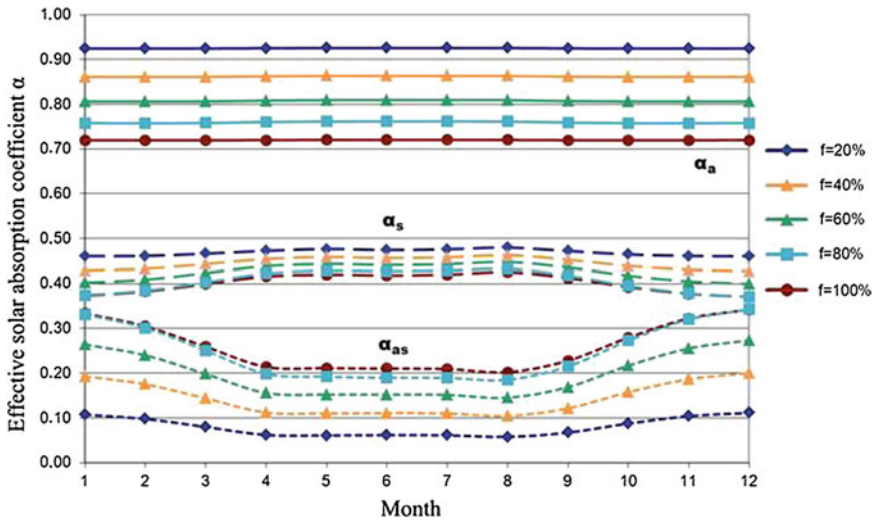


Fig. 12 Average monthly values of the absorption coefficient of the windowed environment α_a , of the environment with sunspace in front α_{as} and of the sunspace α_s , varying the glazed fraction f . Cosenza, southern exposure, $\alpha_f = \alpha_w = 0.2$

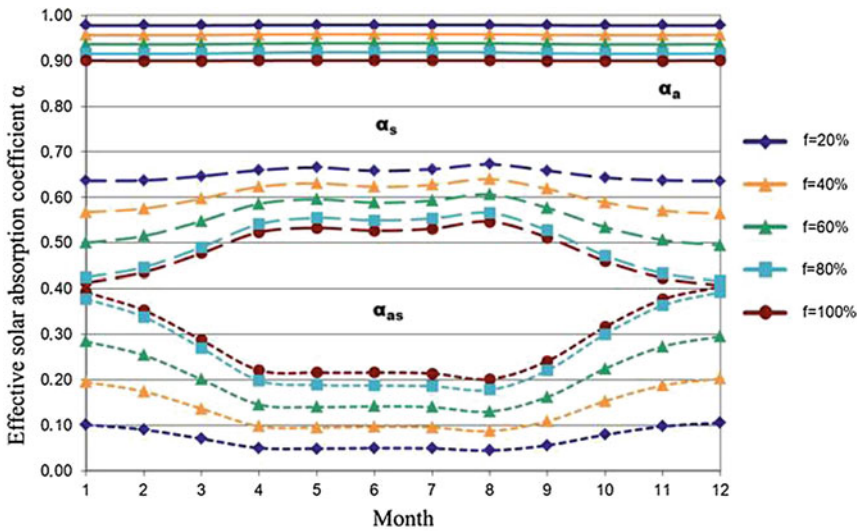


Fig. 13 Average monthly values of the absorption coefficient of the windowed environment α_a , of the environment with sunspace in front α_{as} and of the sunspace α_s , varying the glazed fraction f . Cosenza, southern exposure, $\alpha_f = \alpha_w = 0.5$

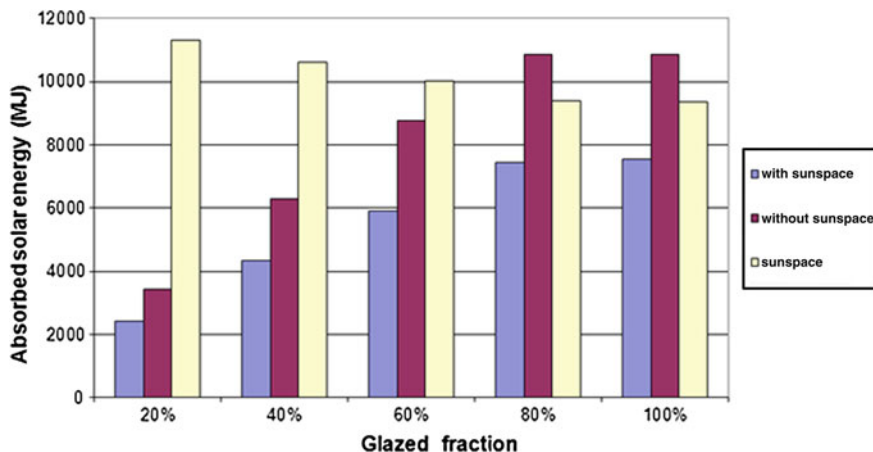


Fig. 14 Solar energy absorbed, during the heating period, by the environment, by the environment with the sunspace and by the sunspace, varying the glazed fraction. Cosenza, southern exposure, $\alpha_f = \alpha_w = 0.2$

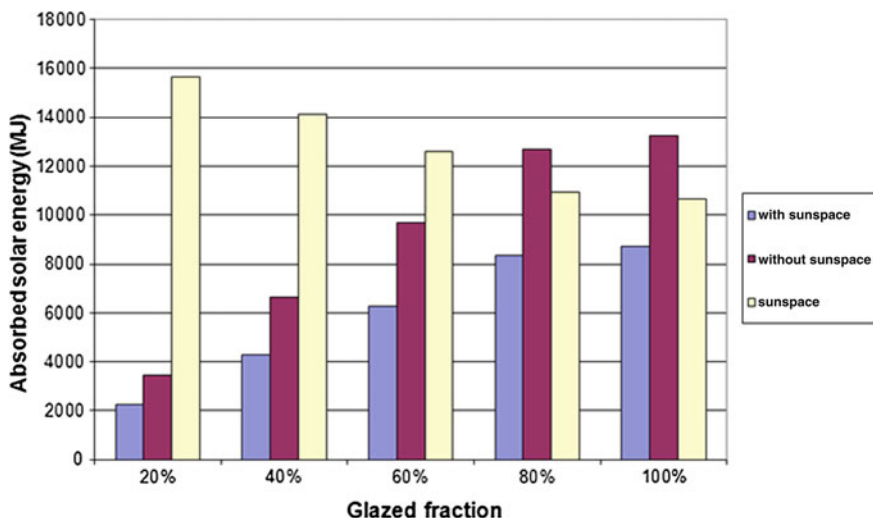


Fig. 15 Solar energy absorbed, during the heating period, by the environment, by the environment with the sunspace and by the sunspace, varying the glazed fraction. Cosenza, southern exposure, $\alpha_f = \alpha_w = 0.5$

with the absorption coefficient of the opaque surfaces and with a reduction in the glazed fraction of the dividing wall.

The prior optical analysis was repeated considering the sunspace located in Milan. The environment, in the absence of a sunspace, presents monthly absorption coefficient values which do not deviate significantly. In winter months, in the

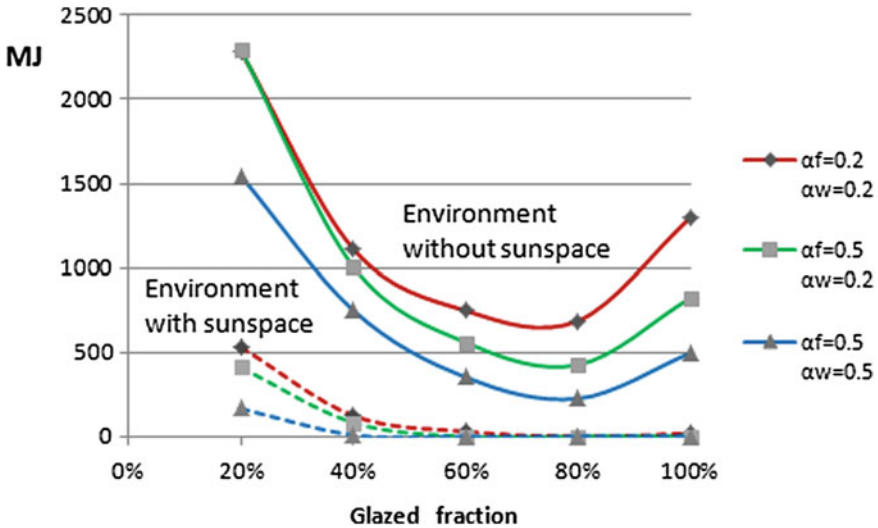


Fig. 16 Seasonal thermal requirements of the environment in the absence and presence of a sunspace, varying the glazed fraction and the optical properties of the opaque surfaces. Cosenza, southern exposure

presence of the sunspace, the environment has absorption coefficients that are about 10 % higher only in the case of environments that are moderately absorbent, while during summer months, the variations are negligible. With regard to the sunspace, the absorption coefficient can be held to be little varied with the location.

For eastern exposure, in the same conditions, the environment absorption coefficient does not present significant variations compared to the southern exposure just described, with a more contained monthly variability, as already highlighted for Cosenza.

If the energy absorbed by the environment in the presence of the sunspace is considered, the comparison, in the same optical conditions, shows a reduction in energy in Milan compared to Cosenza, which is different for higher glazed fractions. For example, for an environment with $\alpha_f = 0.5$ and $\alpha_w = 0.2$, for a glazed fraction $f = 20\%$, the reduction in absorbed energy is equal to 32 %, both for Cosenza and for Milan. With a glazed fraction $f = 100\%$, for Cosenza, there is a decrease of 34 % and for Milan a decrease of 44 %. For eastern exposure, for both localities, the reduction in absorbed energy determined by the presence of the sunspace is around 30 %, independently of the glazed fraction.

With regard to the energy requirements of the environment, in the absence of solar radiation shading systems and sunspace ventilation, with reference to the entire heating period, the results can be summarised as follows. In Fig. 16, the thermal requirements in the absence and presence of a sunspace are compared for the southern exposure.

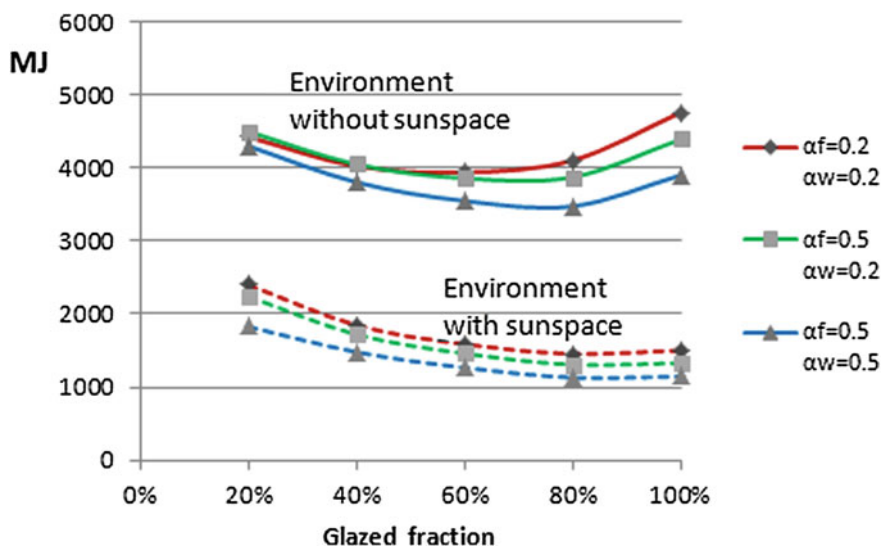


Fig. 17 Seasonal thermal requirements of the environment in the absence and presence of a sunspace, varying the glazed fraction and the optical properties of the opaque surfaces. Cosenza, eastern exposure

The presence of the sunspace requires the use of glazed fractions in the environments that do not exceed 20 % in order to avoid overheating of the environment. Such a fraction ensures a significant reduction in the winter thermal requirement of between 84 %, for reflective environments, and 89 % for environments which are more absorbent. Higher glazed fractions drastically reduce the required thermal requirement.

For eastern exposure, the trend of the environment thermal requirements is reported in Fig. 17. The reduction in the requirements is little influenced by the optical properties of the environments, and increasing the glazed fraction from 20 to 100 %, it varies between 35 and 85 %.

The figures relating to the entire period of heating (15/10–15/04) for Milan are shown in Figs 18 and 19.

The insertion of the sunspace produces important reductions in the winter thermal requirement of between 37 and 60 % for the southern exposure and between 27 and 50 % for the eastern exposure.

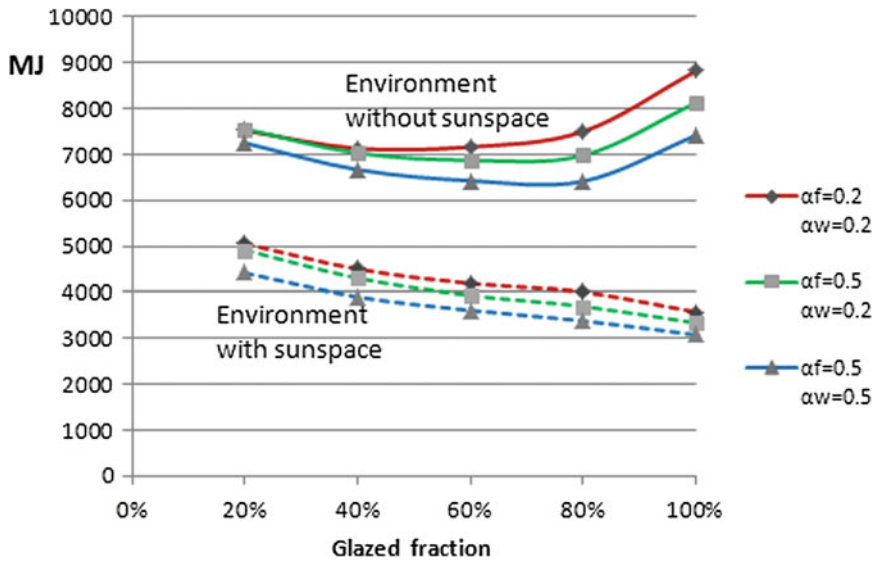


Fig. 18 Seasonal thermal requirements of the environment in the absence and presence of a sunspace, varying the glazed fraction and the optical properties of the opaque surfaces. Milan, southern exposure

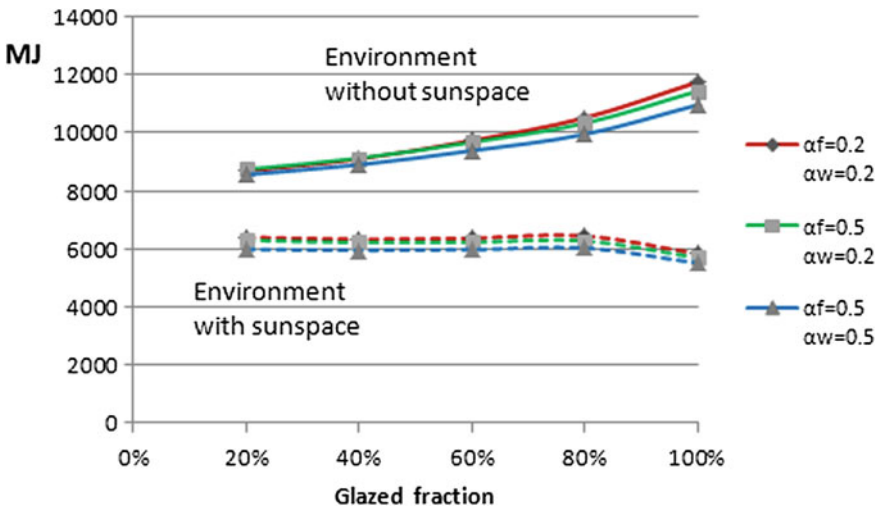


Fig. 19 Seasonal thermal requirements of the environment in the absence and presence of a sunspace, varying the glazed fraction and the optical properties of the opaque surfaces. Milan, eastern exposure

7.3 Sunspaces for Energy Requalification of a Housing Unit in an Apartment Block

The energy advantages offered by sunspaces in a requalification intervention on an existing building are evaluated. The structure is an apartment block situated in the city of Cosenza and was built in 1973. The building has seven floors, the ground floor is used for commercial premises and the six floors above are for residential use. Four housing units are present on each floor, with a surface which varies between 110 and 140 m². The façades are complicated by the presence of terraces, three for each apartment.

Reference was made to one housing unit, the plan of which is reported in Fig 20, situated on a middle floor with a southern and eastern exposure. The net surface on the architectural drawing is 126 m², with an inter-floor height of 2.70 m; it has three balconies of which two are embedded and one overhanging, all with brick parapets. In particular, the south-facing balcony has a surface area in architectural drawings of 8 m²; those with eastern exposure have a surface area equal to 7 and 5.50 m².

The perimeter walls, which are hollow walls, have a thickness of 42 cm and a thermal transmittance of 0.95 W/(m² K); the windows, with wooden frames and single glazing, present a thermal transmittance of 4.9 W/(m² K); the above-lying rolling shutter boxes and the roller shutters are not insulated. The housing unit is heated with a centralised plant; DHW is produced autonomously by means of a gas boiler.

The energy requalification intervention is obtained through the conversion of the balconies into sunspaces according to two different solutions:

1. Realisation of sunspaces with transparent–opaque systems. It is the least costly and invasive intervention, which foresees the closure of the balconies by means of continuous glazing, maintaining the existing parapets;
2. Removal of the brick parapets in order to realise a system of sunspaces which are completely transparent, both in the lower part, which remains fixed, and in the upper part which can be opened.

The energetic benefits are calculated by means of the evaluation of the reduction in the winter thermal requirement obtained through thermal simulations in dynamic regime [16].

Figures 21 and 22 illustrate the two intervention hypotheses. Two solutions were considered for the realisation of the sunspaces: the use of clear single glazing 6 mm and of clear double glazing 4–12–4 mm.

In Table 13, the seasonal values of the thermal heating requirement of the housing unit in absence of and presence of the sunspace are presented. All the considered solutions give rise to a significant saving, which is variable between 31 and 41 %. The presence of double glazing offers better results, both in the absence and in the presence of the parapet.

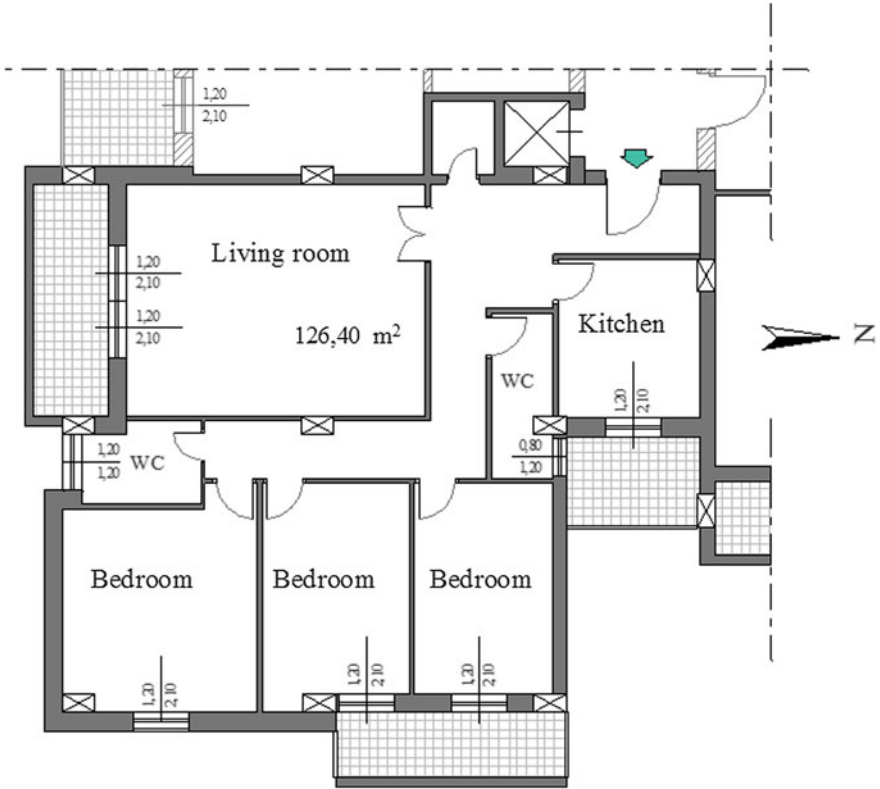


Fig. 20 Architectural drawing of dwelling with southeastern exposure

Fig. 21 Sunspaces with a mixed glass–opaque shell (solution 1)





Fig. 22 Sunspaces with an entirely glazed shell (solution 2)

Table 13 Thermal requirement of the housing unit for the heating period and reduction in percentage of the energy requirement for different intervention solutions

		Energy requirement for winter heating (kWh/m ²)	Reduction in energy requirement produced by sunspace (%)
Housing unit without sunspace		37.19	
Transparent–opaque shell	Single glazing (6 mm)	25.69	31
	Double glazing (4–12–4 mm)	23.82	36
Transparent shell	Single glazing (6 mm)	24.58	34
	Double glazing (4–12–4 mm)	21.76	41

8 Phase Change Materials

Nowadays, there is a tendency to realise buildings with light materials and small envelope thickness, so as to reduce the weight, the cost of transport and the time for construction. Unfortunately, these modern lightweight buildings suffer from pronounced overheating in summer, especially those characterised by large glazed surfaces, hence by important solar gains.

In order to compensate for the small storage capacity of lightweight buildings, the incorporation of phase change materials (PCMs) into the opaque envelope can be an effective way to enhance thermal inertia and to improve the energy performance, both in the construction stage and during refurbishment.

Indeed, thanks to their high latent heat, PCMs can store a significant amount of thermal energy at daytime while melting, thus reducing the indoor air temperature swings produced by solar and internal gains. At night, thermal energy is released and the material can restore its solid state; this stage can be enhanced by ventilating the building with fresh outdoor air.

Organic PCMs, such as paraffin, fatty acids and polyethylene glycol (PEG), are the most frequently used materials; they show good chemical stability, high latent heat and very limited super-cooling. Unfortunately, they have low thermal conductivity, which may reduce the penetration of the thermal wave into the core of the material and the full exploitation of its latent heat. Moreover, the majority of the common paraffinic PCMs are flammable, and they may not meet the strict low-flammability criteria set by the American Society for Testing Materials (ASTM). Possible solutions to limit flammability through the addition of fire retardants are discussed in Ref. [17].

The simplest and most widespread way of using PCM in buildings consists in their impregnation into gypsum, concrete or other porous materials. However, micro-encapsulation techniques have been recently developed: they consist in enclosing the PCM in microscopic polymer capsules that form a sort of powder; the powder is then included in a container made up of PVC or aluminium [18]. The final product is generally distributed as a panel or wallboard, easy to be handled and installed, from which the PCM cannot leak; furthermore, the reduced size of the microcapsules enhances the full exploitation of the PCM, because of the large surface available for heat exchange, thus optimising its effectiveness. A detailed review about the most common PCMs and the technical solutions for application in buildings can be found in [19, 20].

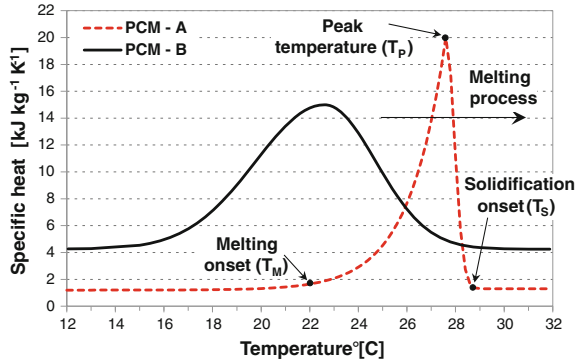
In order to provide a comprehensive view about the use of micro-encapsulated PCM wallboards for refurbishing lightweight buildings, so as to reduce the overheating due to solar gains, a case study is considered in the following, based on the dynamic thermal simulation of a sample building. The study will be extended to different climates in Europe and will highlight the essential role of night ventilation to maximise the effectiveness of this solution.

Moreover, with the aim of making the study more general, two different PCM wallboards will be considered.

The first wallboard (PCM-A) includes an aluminium honeycomb matrix, filled with a compound containing 60 % of a paraffin wax, encapsulated within polymeric microspheres with a diameter of approximately 5 μm . The wallboard is sealed by two thin aluminium sheets, and its overall thickness is 20 mm, as described by Ref. [21]. The weight of the wallboards is around 11 kg/m^2 .

The second wallboard (PCM-B) is made of a micro-encapsulated paraffin, different from the previous one, as described later. The final form of this wallboard is a flexible panel with a thickness of 5.26 mm, covered on both sides with a very thin aluminium sheet [22]; the final weight is 4.5 kg/m^2 .

Fig. 23 Curves of the equivalent specific heat capacity for the two proposed PCMs



8.1 Characterisation of the Phase Change Materials

The melting process of a PCM used for building applications does not entirely occur at a given temperature, as for pure PCMs, but it is completed over a certain temperature range. In order to quantify the amount of heat absorbed by a PCM wallboard during phase change, the *equivalent specific heat capacity* C_{eq} is used. This parameter represents the thermal energy needed to produce a unit temperature variation of the unit mass of PCM at constant pressure:

$$C_{eq}(T) = \frac{\partial h(T)}{\partial T} \quad (52)$$

As a rule, the evaluation of C_{eq} is performed through laboratory tests, by imposing a periodic temperature fluctuation to a PCM sample and then measuring its enthalpy variation. The equivalent heat capacity normally fits a Gaussian curve, with a maximum value occurring at the peak melting temperature T_p . As an example, Fig. 23 shows the curves of the equivalent heat capacity of the two PCMs mentioned above; the corresponding mathematical formulation is reported in Ref. [23] and Ref. [24], respectively.

As one can observe, the melting process of PCM-A starts at $T_m = 22$ °C and is completed at $T_s = 28.5$ °C; the peak temperature is $T_p = 27.6$ °C, after which melting is achieved quite rapidly. Actually, according to the laboratory tests, the profile of the equivalent heat capacity during the solidification phase is slightly different, as the solidification starts at around 28 °C and the peak of the curve would occur at around 27.2 °C. Hence, the curve of the equivalent specific heat capacity for cooling/solidification is somewhat shifted towards lower temperatures if compared to that determined for the melting phase.

This behaviour, called *super-cooling*, is quite typical for paraffin, but it cannot be easily modelled by most of the programs used for the dynamic thermal simulation of buildings. However, Tabares-Velasco et al. demonstrated that the impossibility of simulating super-cooling does not affect significantly the reliability of the results [25].

On the other hand, the behaviour of PCM-B is considerably different. In fact, the melting process is distributed over a wider temperature range than for PCM-A (from $T_m = 17\text{ }^\circ\text{C}$ to $T_s = 27\text{ }^\circ\text{C}$), but the highest value of the equivalent heat capacity is lower than for PCM-A. Furthermore, the lower peak temperature ($T_p = 22.6\text{ }^\circ\text{C}$) suggests that the exploitation of this PCM should benefit from lower indoor temperatures.

Another important parameter that characterises a PCM is the thermal conductivity; in the case of PCM-A, the measured effective thermal conductivity is $2.7\text{ W}/(\text{m K})$. This value is remarkably high, if compared to PCM-B, whose thermal conductivity varies between 0.18 and $0.22\text{ W}/(\text{m K})$. This difference is imputable to the aluminium honeycomb matrix, which allows heat to be easily transferred through the panel.

On the whole, the latent heat of both PCM wallboards, i.e. the thermal energy needed to complete the whole melting process from T_m to T_s , is very similar when referred to the unit surface, as it amounts to $131.7\text{ Wh}/\text{m}^2$ and to $134.0\text{ Wh}/\text{m}^2$, respectively, for PCM-A and PCM-B.

8.2 Case Study

Figure 24 shows the sample building considered in this investigation: it is conceived as a module of a typical office building, with a large glazed surface protected by movable blinds, a concrete frame, a well-insulated envelope and very light partition walls to separate the different offices. This typology of buildings normally suffers from significant overheating in summer; thus, a good strategy for its refurbishment could be the application of PCM wallboards on the inner surface either of the partition walls or of the ceiling, thus enhancing the building thermal inertia.

The main façade of the building is due southwest; the size of each room is 5 m by 3.5 m , with a height of 2.5 m . Floors and ceilings are made of a non-insulated concrete slab as thick as 200 mm ; the internal partitions are composed of two plasterboards with a 40-mm layer of glass wool in between. The façade has a 100-mm layer of heavyweight concrete, with an outermost layer of glass wool (70 mm). The windows are provided with an aluminium frame (10 cm in width) and a 4-16-4 double glazing with air filling. External venetian blinds are also available; these are kept open during the simulations, unless the incident solar radiation on the glazing gets higher than $250\text{ W}/\text{m}^2$. The space behind the rooms at each floor is occupied by a large corridor and by a series of identical rooms facing northeast.

As far as ventilation is concerned, a constant air change rate $n = 0.5\text{ h}^{-1}$ is considered for hygienic purposes. In order to check the effect of night ventilation on the performance of the PCM wallboards, an additional night ventilation rate is introduced between 21:00 and 06:00, with an air change rate $n = 4\text{ h}^{-1}$ or $n = 8\text{ h}^{-1}$.

The simulations needed for this study are carried out on EnergyPlus version 7.0 over the summer period (June–September). Firstly, the weather data of Milan (Lat.

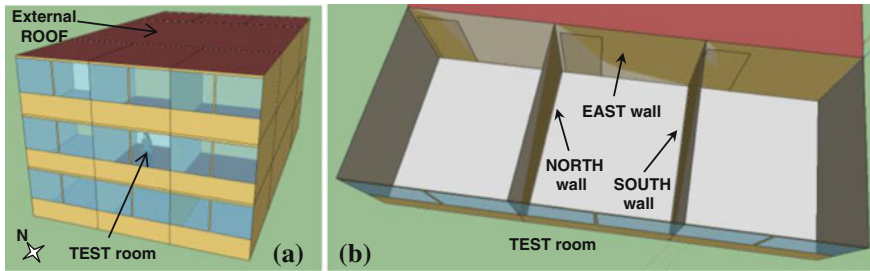


Fig. 24 **a** Model of the simulated building and **b** partitions fully covered with PCM wallboards

Table 14 Main data concerning the test room in the simulated model

Floor surface	17.5 (m ²)
Window size	1.5 × 1.7 (m ²)
Room volume	43.7 (m ³)
Partition wall: <i>U</i> -value	2.7 (W/(m ² K))
External wall: <i>U</i> -value	0.68 (W/(m ² K))
Floor/ceiling: <i>U</i> -value	2.8 (W/(m ² K))
Glass <i>U</i> -value	2.7 (W/(m ² K))
Glass <i>g</i> -value	0.76 (-)
Occupancy rate	0.12 (people/m ²)
Occupancy time	08:00–18:00
People sensible thermal load	60 (W/person)
Electric appliances	100 (W)
Lights	8 (W/m ²)

45°27'N, Italy) will be used, as an example of continental climate; in a second stage, other locations in Europe will be considered.

Three series of simulations are performed: the first one without PCM wallboards and the others with the PCM wallboards placed in the test room, respectively:

1. on the inner faces of the three partition walls,
2. on the inner surface of the ceiling, as shown in Fig. 24.

The main data used to build the simulated model are reported in Table 14.

8.3 Results and Discussion

In most of the research works available in the scientific literature and regarding the use of PCM wallboards for improving summer thermal comfort in buildings, the effectiveness of PCMs is measured by the indoor temperature drop achieved, during a short representative period, thanks to the application of the PCM, in comparison with the case without PCM. However, it is to remark that the room

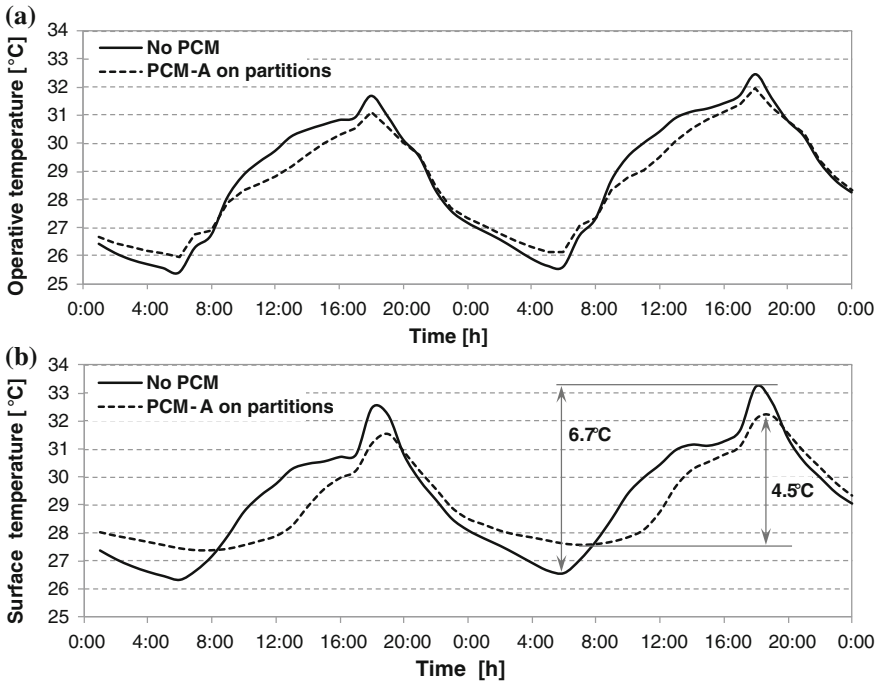


Fig. 25 Effect of PCM-A on the operative temperature (a) and the surface temperature of the south wall (b), when the night air change rate is $n = 4 \text{ h}^{-1}$

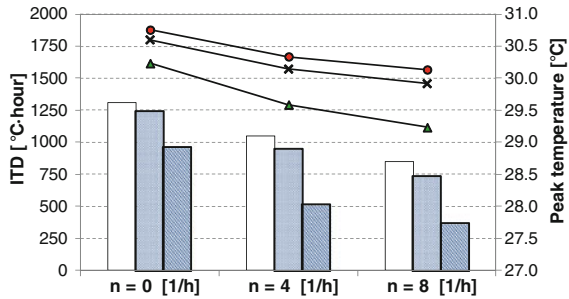
operative temperature, and not the indoor air temperature, is the parameter that directly affects the comfort sensation, as suggested by well-established comfort theories, reported in the International Standards ISO 7730 [31] and EN 15251 [32]. According to this approach, the discussion of the results will be based on the values of the operative temperature obtained from the simulations.

8.3.1 Results

The profile of the indoor operative temperature in the test room with and without PCM for two sunny days in July is shown in Fig. 25a. Both curves refer to the case with $n = 4 \text{ h}^{-1}$; in the case with PCM, the wallboards containing PCM-A are applied on the inner surface of all the partition walls.

The figure shows that the installation of the PCM wallboards yields a reduction in the peak operative temperature of about $0.7 \text{ }^\circ\text{C}$, but in the central hours of the day, this difference keeps around $1.0 \text{ }^\circ\text{C}$ for almost 3 h. In addition, Fig. 25b shows a significant attenuation in the daily surface temperature swing of the partitions when using PCM: as an example, the peak surface temperature of the south wall drops from 33.2 to $32.1 \text{ }^\circ\text{C}$ during the second day, and the daily

Fig. 26 Comparison based on the ITD and the average peak operative temperature, measured over the whole summer season in Milan



temperature swing is reduced from 6.7 to 4.5 °C. Finally, a slight time shift of the peak surface temperature can be observed, which is another visible effect of the additional thermal inertia provided by the PCM.

Methodological remarks

However, in the attempt of having a more comprehensive view about the effect of PCMs on thermal comfort, a deeper analysis is requested. To this aim, an effective way to quantify the uncomfortable thermal sensation due to overheating might be the measure of the difference between the operative temperature and a threshold value for it. On this basis, the indicator called *Intensity of Thermal Discomfort* (ITD) can be adopted: it is defined as the time integral, over the occupancy period P , of the positive difference between the current operative temperature and the upper threshold for comfort [23]:

$$ITD = \int_P (T_{op}(\tau) - T_{lim})^+ d\tau \quad (53)$$

Thus, the ITD measures at the same time the intensity and the duration of the thermal discomfort perceived by the occupants. The value of the threshold temperature T_{lim} depends on the choice of a specific thermal comfort theory. In this work, the adaptive approach is used, as described in the EN 15251 Standard [32]; hence, the threshold value is not constant in time, but it is determined daily as a function of the running mean outdoor air temperature [26].

Further results

At this point, the new indicators introduced so far can be used to provide some more information about the effectiveness of the wallboards containing PCM-A. In particular, the aim is to underline the role of the night ventilation as well as the effect of the position of the wallboards. The results of this analysis are reported in Fig. 26.

The first message conveyed by Fig. 26 is that the PCM wallboards are far more efficient if applied on the partition walls than on the ceiling. As an example, with reference to $n = 4 \text{ h}^{-1}$, the application of PCM-A on the partition surface would yield a reduction of 51.5 % in the seasonal ITD if compared to the case without PCM, whereas such improvement would only amount to 8.9 % in the case of the ceiling. The difference between the two cases is remarkable.

Moreover, in terms of average peak operative temperature, the attenuation introduced by the PCM wallboards, still under the hypothesis $n = 4 \text{ h}^{-1}$, would be 0.7 and 0.2 °C, respectively, with the PCM applied either on the inner walls or on the ceiling. These results can be partially justified by the larger surface area available on the partitions (27 m²) than on the ceiling (17.5 m²). However, it is also to remark that the partitions—but not the ceiling—are directly hit by the solar radiation during the day; this determines a faster and more intense melting of the PCM, hence a more effective exploitation of its latent heat. One more simulation was devoted to the case where all the surfaces are covered by PCM (partitions plus ceiling), and the results were very close to those obtained with the PCM only on the partitions walls.

Another key message emerging from the simulations is the importance of a good night ventilation strategy that boosts the discharge of the heat absorbed during daytime. Actually, Fig. 26 shows that the peak temperature is relatively sensitive to the night ventilation rate, but even more sensitive to n is the ITD.

However, it can be observed that a saturation effect occurs; thus, it is not recommendable to go beyond $n = 8 \text{ h}^{-1}$, since the benefit on both the peak operative temperature and the ITD tends to vanish. It is also understood that such intense ventilation can only be practised in tertiary buildings that are supposed to be not occupied at night; furthermore, if the ventilation is procured by mechanical means, an accurate calculation of the electricity consumption should be done to avoid severe penalties to the benefits discussed so far.

8.3.2 Correlation Between Climate and PCM Effectiveness

The results reported in the previous section suggest that the wallboards containing PCM-A can allow a significant improvement in the indoor thermal comfort in a room of a typical lightweight office building located in Milan (Italy, continental climate).

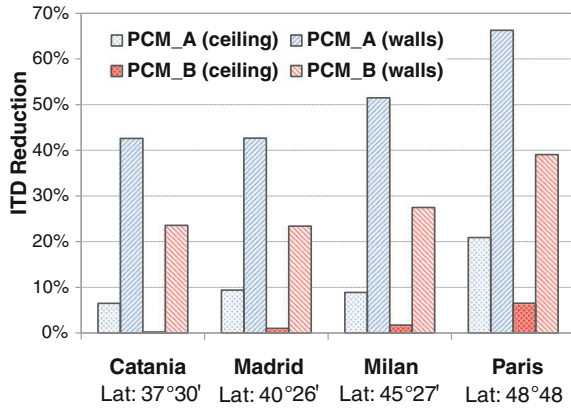
Now, it is interesting to investigate whether such favourable outcomes hold true also in other climatic contexts; furthermore, the effectiveness of PCM-B in place of PCM-A has to be examined. The main results of this analysis are reported in Fig. 27 and will be discussed hereafter.

Effect of the climatic conditions

As shown in Fig. 27, the effectiveness of PCM-A in reducing the ITD in the test room is not the same for all the sites considered. Apparently, a certain correlation emerges between the ITD reduction and the latitude of the site. Indeed, the highest values of the ITD reduction occur in northern Europe (66.2 %, Paris), whereas the least satisfying results are those concerning southern Europe: around 42 % in Catania (Southern Italy) and Madrid (Spain). In addition, an average effectiveness of the PCM is observed in central Europe (51.5 %, Milan), as already remarked in Fig. (26).

Such a tendency can be easily justified if one thinks that the high values of the solar irradiance occurring in summer at low latitudes induce an intense PCM melting at daytime. Then, at night, as the outdoor air temperature is on average

Fig. 27 Reduction in the ITD, thanks to the application of PCM wallboards on the room surfaces (all cases refer to $n = 4 \text{ h}^{-1}$)



quite high, there is a low potential for refreshing the room and discharging the heat absorbed by the PCM, which cannot be completely solidified. On the contrary, at high latitudes, the PCM melting process might be often not complete, whereas solidification at night is easily achieved. In any case, the PCM installed on the ceiling is far less effective than when applied on the partitions, whatever the latitude of the site.

Comparison between different PCMs

The results reported in Fig. 27 also show that the wallboards containing PCM-B are not as effective as PCM-A in reducing the intensity and the duration of the thermal discomfort perceived in the test room.

As an example, in the case of the PCM wallboards applied on the partitions, the reduction in the ITD remarked in Paris in comparison with the case without PCM is 66.3 % for PCM-A and only 39.1 % for PCM-B. Similar trends emerge in the other sites, as well as when the PCM is applied on the ceiling.

Here, one can observe that the phase change for PCM-B occurs over a range of temperatures quite lower than for PCM-A (see Fig. 23). Hence, in the presence of the high temperatures usually measured in summer in freerunning lightweight buildings, the storage capacity of PCM-B cannot be exploited as effectively as for PCM-A. Further investigations on this point are presented in the following.

8.3.3 The PCM Storage Efficiency

In order to assess more accurately the performance of a PCM, it is necessary to understand whether and to what extent its latent heat is effectively exploited. To this aim, it can be useful to calculate the *Frequency of Activation* (FA), i.e. the percentage of time within a given period during which the PCM is actually undergoing phase change [23]. This occurs between $T_m = 22 \text{ °C}$ and $T_s = 28.5 \text{ °C}$ for PCM-A, and in the range $17 \text{ °C} - 27 \text{ °C}$ for PCM-B (see Fig. 23).

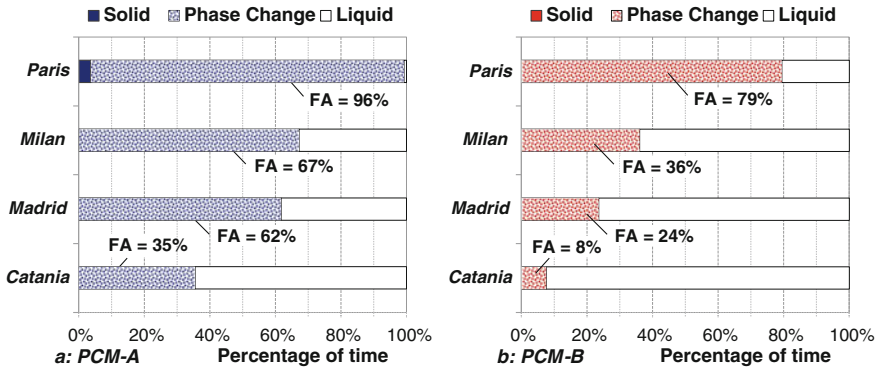


Fig. 28 Average FA of the PCM wallboards (July and August, $n = 4 \text{ h}^{-1}$)

The FA can provide important information: when its value is low, it means that the PCM remains in its liquid or solid phase for a long time; thus, its latent heat capacity is not exploited. An ideal application of a PCM should imply $FA = 100 \%$, but this is not easy to accomplish, as the activation of the PCM is highly influenced by many circumstances.

The results obtained for the sample building in terms of FA are shown in Fig. 28. Here, it is possible to observe that the wallboards containing PCM-A seem to work very well in Paris, as the PCM is almost always activated throughout the season ($FA = 96 \%$). On the contrary, the same wallboards keep very often in the liquid phase if installed in Catania, where the FA is much lower than in other sites ($FA = 35 \%$), due to the severe climatic conditions in summer. As concerns PCM-B, its FA is always far lower than for PCM-A.

However, not all the conditions inside the melting range have the same importance from an energetic point of view. In other words, the heat capacity of a PCM is strongly dependent on temperature: as an example, the equivalent specific heat capacity of PCM-A at the peak temperature $T_p = 27.6 \text{ }^\circ\text{C}$ is almost 5 times as high as at $25 \text{ }^\circ\text{C}$, and vice versa. Consequently, at $25 \text{ }^\circ\text{C}$, the PCM-A, despite being activated, has a storing capacity 5 times lower than at $T_p = 27.6 \text{ }^\circ\text{C}$. Nevertheless, the FA itself is obviously not capable of accounting for this difference.

Therefore, it appears suitable to introduce a new indicator called PCM storage efficiency that measures the ratio of the thermal energy actually stored by the PCM to its maximum storage capacity, i.e. its latent heat L , as defined in Eq. (54). Since the PCM is subject to daily temperature cycles, the actual energy storage must be evaluated over the period $P = 24 \text{ h}$ [23].

$$\eta_{\text{PCM}} = \frac{E_{\text{st}}}{L} = \frac{\int_P \left(M \cdot C_{\text{eq}} \cdot \frac{dT_{\text{PCM}}}{d\tau} \right) d\tau}{\int_{T_m}^{T_s} M \cdot C_{\text{eq}}(T) dT} \tag{54}$$

Table 15 Average values of the PCM storage efficiency (July and August, $n = 4 \text{ h}^{-1}$)

	PCM type A		PCM type B	
	On walls	On ceiling	On walls	On ceiling
Catania	35.0 %	9.9 %	19.7 %	7.6 %
Madrid	41.0 %	14.0 %	19.9 %	7.6 %
Milan	42.1 %	14.6 %	24.4 %	9.4 %
Paris	42.6 %	20.7 %	35.1 %	13.9 %

The average values of the daily PCM storage efficiency η_{PCM} are reported in Table 15. Here, a distinction is also made between the wallboards applied on the partitions and those installed on the ceiling. The values of this indicator are usually significantly lower than FA: as an example, the average storage efficiency is $\eta_{\text{PCM}} = 42.6 \%$ for PCM-A in Paris, even if the PCM turns out to be activated for more than 90 % of time (FA = 96 %). Very low values of η_{PCM} occur for PCM-B, ranging from 19.7 to 35.1 % when installed on walls and from 7.6 to 13.9 % when installed on the ceiling. According to these figures, the effectiveness of the PCM wallboards seems not to be very satisfying, despite their frequent activation. The reason for this apparently reduced PCM potential can be found by looking at Fig. 29, where each point describes the mean operating conditions of a wallboard throughout a day in summer.

The highest values of the daily storage efficiency of PCM-A (between 60 and 70 %, see Fig. 29a) pertain to those days where the average temperature of the PCM wallboards is very close to the peak melting temperature. This corresponds to what already remarked by Neepser [27]. However, such a condition occurs only occasionally in July and August; on the contrary, the daily temperature of the PCM is frequently either too low (in Paris) or too high (in Catania). As a general rule, the farther from T_p is the daily average PCM temperature, the lower is the daily PCM storage efficiency.

When looking at PCM-B, the situation is more unsatisfying: here, all points regarding Catania are very close to the upper limit of the melting range; thus, the daily storage efficiency always keeps between 15 and 25 % (see Fig. 29b). Better results are observed in Paris; nevertheless, the daily values of η_{PCM} hardly exceed 50 %.

The indications coming out from this analysis are coherent with the results reported in Fig. 27. This confirms that the ability of a PCM wallboard to improve summer thermal comfort in lightweight buildings is strictly related to the possibility of exploiting its latent heat capacity; this implies the need of keeping its temperature very close to the peak melting temperature T_p as long as possible. To this aim, different techniques are currently being investigated, mostly based on the improvement of the heat transfer coefficient between indoor air and PCM wallboard.

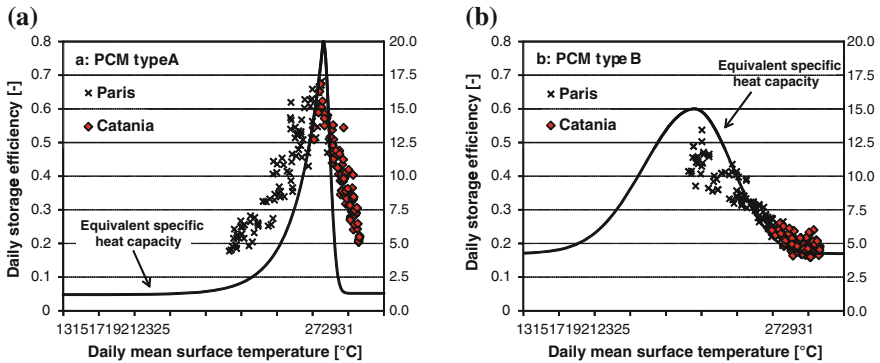


Fig. 29 Average daily PCM temperature versus average daily storage efficiency. Each point represents the mean value for all partitions (July and August, $n = 4 \text{ h}^{-1}$)

As a conclusion, the convenience of PCMs in buildings must be carefully considered, also in relation to the local climate. The main parameters that affect the PCM effectiveness are as follows:

1. the position of the PCM wallboard within the room,
2. the rate of ventilation at night, and
3. the value of the peak melting temperature for the specific PCM.

References

1. Kreith F, Kreider JF (1978) Principles of solar engineering. McGraw-Hill, New York
2. Duffie JA, Beckman WA (2006) Solar engineering of thermal processes, 3rd edn. Wiley, New York
3. Cucumo MA, Marinelli V, Oliveti G (1994) Ingegneria solare principi and applicazioni (principles and applications of solar engineering). Pitagora, Bologna
4. Eicher U (2003) Solar technologies for buildings. Wiley, England
5. Oliveti G, Arcuri N, Bruno R, De Simone M (2011) Sistemi solari nella riqualificazione energetica degli edifici (solar systems for the buildings energy requalification). National Journal La Termotecnica 5
6. Evans DL (1981) Simplified method for predicting photovoltaic array output. Sol Energy 27:555
7. Biagini MV, Lorenzini G, Saro O (2012) The evolution of photovoltaic technologies for energy production: state-of-the-art context and recent developments. Int J Energ Technol 4(6):1–11
8. Coiante D (2009) Le Nuovi Fonti di Energia Rinnovabile (The new sources of renewable energy). Franco Angeli, Milano
9. Siegel MD, Klein SA, Beckman WA (1981) A simplified method for estimating the monthly-average performance of photovoltaic systems. Sol Energy 26:413
10. Clark DR, Klein SA, Beckman WA (1984) A method for estimating the performance of photovoltaic systems. Sol Energy 33:551
11. Cucumo MA, Kaliakatsos D, Marinelli V (1993) Sul Calcolo del Coefficiente di Trasmissione Solare delle Superfici Vetrare (On the calculation of the solar transmission coefficient of glazed surfaces). In: Proceedings of the 48° National Conference A.T.I

12. Utzinger MD, Klein SA (1979) A method of estimating monthly average solar radiation on shaded receivers. *Sol Energy* 23:369
13. Oliveti G, Arcuri N, Bruno R, De Simone M (2011) An accurate calculation model of solar heat gain through glazed surfaces. *Energy Build* 43:269–274
14. Oliveti G, De Simone M, Ruffolo S (2008) Evaluation of the absorption coefficient for solar radiation in sunspaces and windowed rooms. *Sol Energy* 82:212–219
15. Oliveti G, Arcuri N, De Simone M, Bruno R (2012) Solar heat gains and operative temperature in attached sunspaces. *Renew Energy* 39:241–249
16. DEROB-LTH v1.0. (2004) User's manual. Division of Energy and Building Design, Lund Institute of Technology, Sweden
17. Sittisart P, Farid MM (2011) Fire retardants for phase change materials. *Appl Energy* 88:3140–3145
18. Tyagi VV, Kaushik SC, Tyagi SK, Akiyama T (2011) Development of phase change materials based microencapsulated technology for buildings: a review. *Renew Sust Energ Rev* 15:1373–1391
19. Rodriguez-Ubinas E, Ruiz-Valero L, Vega S, Neila J (2012) Applications of phase change materials in highly energy-efficient houses. *Energy Build* 50:49–62
20. Soares N, Costa JJ, Gaspar AR, Santos P (2013) Review of passive PCM latent heat thermal energy storage systems towards buildings' energy efficiency. *Energy Build* 59:82–103
21. Hasse C, Grenet M, Bontemps A, Dendievel R, Sallée H (2011) Realization, test and modelling of honeycomb wallboards containing a phase change material. *Energy Build* 43:232–238
22. Kuznik F, Virgone J, Roux JJ (2008) Energetic efficiency of room wall containing PCM wallboard: a full-scale experimental investigation. *Energy Build* 40:148–156
23. Evola G, Marletta L, Sicurella F (2013) A methodology for investigating the effectiveness of PCM wallboards for summer thermal comfort in buildings. *Build Environ* 59:517–527
24. Kuznik F, Virgone J (2009) Experimental assessment of a phase change material for wall building use. *Appl Energy* 86:2038–2046
25. Tabares-Velasco PC, Christensen C, Bianchi M (2012) Verification and validation of EnergyPlus phase change material model for opaque wall assemblies. *Build Environ* 54:186–196
26. Sicurella F, Evola G, Wurtz E (2012) A statistical approach for the evaluation of thermal and visual comfort in free-running buildings. *Energy Build* 47:402–410
27. Neeper DA (2000) Thermal dynamics of wallboard with latent heat storage. *Sol Energy* 68:393–403

Reference Standards

28. EN 15316-4-3 (2007) Heating systems in buildings—Method for calculation of system energy requirements and system efficiencies—Part 4–3: Heat generation systems, thermal solar systems
29. EN 410 (2011) Glass in building—Determination of luminous and solar characteristics of glazing
30. EN ISO 13790 (2008) Energy performance of buildings—Calculation of energy use for space heating and cooling
31. ISO 7730 (2005) Ergonomics of the thermal environment—Analytical determination and interpretation of thermal comfort using calculation of the PMV and PPD indices and local thermal comfort criteria
32. EN 15251 (2007) Indoor environmental input parameters for design and assessment of energy performance of buildings addressing indoor air quality, thermal environment, lighting and acoustics